



1-D steady state runoff production in light of queuing theory: Heterogeneity, connectivity, and scale

Marie-Alice Harel, Emmanuel Mouche

► To cite this version:

Marie-Alice Harel, Emmanuel Mouche. 1-D steady state runoff production in light of queuing theory: Heterogeneity, connectivity, and scale. Water Resources Research, 2013, 49 (12), pp.7973-7991. <10.1002/2013WR013596>. <hal-02887192>

HAL Id: hal-02887192

<https://hal.science/hal-02887192v1>

Submitted on 28 Oct 2020

HAL is a multi-disciplinary open access archive for the deposit and dissemination of scientific research documents, whether they are published or not. The documents may come from teaching and research institutions in France or abroad, or from public or private research centers.

L'archive ouverte pluridisciplinaire **HAL**, est destinée au dépôt et à la diffusion de documents scientifiques de niveau recherche, publiés ou non, émanant des établissements d'enseignement et de recherche français ou étrangers, des laboratoires publics ou privés.



HAL Authorization

1-D steady state runoff production in light of queuing theory: Heterogeneity, connectivity, and scale

M.-A. Harel¹ and E. Mouche¹

Received 26 January 2013; revised 23 October 2013; accepted 26 October 2013; published 5 December 2013.

[1] We used the frameworks of queuing theory and connectivity to study the runoff generated under constant rainfall on a one-dimensional slope with randomly distributed infiltrability. The equivalence between the stationary runoff-runon equation and the customers waiting time in a single server queue provides a theoretical link between the statistical description of infiltrability and that of runoff flow rate. Five distributions of infiltrability, representing soil heterogeneities at different scales, are considered: four uncorrelated (exponential, bimodal, lognormal, uniform) and one autocorrelated (lognormal, with or without a nugget). The existing theoretical results are adapted to the hydrological framework for the exponential case, and new theoretical developments are proposed for the bimodal law. Numerical simulations validate these results and improve our understanding of runoff-runon for all of the distributions. The quantities describing runoff generation (runoff one-point statistics) and its organization into patterns (patterns statistics and connectivity) are studied as functions of rainfall rate. The variables describing the wet areas are also compared to those describing the rainfall excess areas, i.e., the areas where rainfall exceeds infiltrability. Preliminary results concerning the structural and functional connectivity functions are provided, as well as a discussion about the origin of scale effects in such a system. We suggest that the upslope no-flow boundary condition may be responsible for the dependence of the runoff coefficient on the scale of observation. Queuing theory appears to be a promising framework for runoff-runon modeling and hydrological connectivity problems.

Citation: Harel, M.-A., and E. Mouche (2013), 1-D steady state runoff production in light of queuing theory: Heterogeneity, connectivity, and scale, *Water Resour. Res.*, 49, 7973–7991, doi:10.1002/2013WR013596.

1. Introduction

[2] The assessment and prediction of the hydrograph peak flow, soil erosion, and sediment transport during a rainfall event involves an accurate knowledge of runoff formation and spatial organization on one hand, and runoff volume and flow rate on the other. These characteristics in turn depend on the rainfall intensity, land-cover, hillslope topography, and soil parameters such as composition, moisture content, and crusting.

[3] At the plot scale, runoff is generally produced by infiltration excess [e.g., Yu *et al.*, 1997]. The soil surface quickly becomes saturated at the beginning of a rainfall event, and then the volume of rainfall that cannot infiltrate becomes runoff. This process is often called Hortonian

overland flow. Experiments performed under natural or simulated rainfall frequently show that the infiltration rate depends on rainfall intensity [Lafforgue, 1977; Yu *et al.*, 1997; Van Dijk and Bruijnzeel, 2004; Langhans *et al.*, 2011]. Simulated rainfall experiments indicate that the steady state infiltration rate increases with rainfall intensity and becomes constant at high intensities [Paige *et al.*, 2002; Stone *et al.*, 2008]. This observation is inconsistent with Horton's law, which states that the long-term infiltration rate is an intrinsic soil property that does not depend on rainfall [Horton, 1935]. Horton's law is adapted to ideal plots (homogeneous soil, plane surface, no vegetation, and no changes in surface conditions) [e.g., Ribolzi *et al.*, 2011].

[4] Two reasons are put forth in the literature to qualitatively explain the observed rainfall dependency: spatial variability of point infiltration capacity and microtopography [Dunne *et al.*, 1991; Langhans *et al.*, 2011]. At the plot scale, crusts, vegetation cover, microtopography, and their combined effects lead to a heterogeneous soil surface with a large range of point infiltration capacities. When the rainfall rate increases, the fraction of the plot area for which infiltration capacity is smaller than the rainfall rate also increases. As a result, the apparent steady state infiltration rate (the sum of the point infiltration rates divided by the plot area) is an increasing function of the rainfall rate. In terms of microtopography, it has been observed that

Additional supporting information may be found in the online version of this article.

¹Laboratoire des Sciences du Climat et de l'Environnement, CEA-CNRS-UVSQ, Gif-sur-Yvette, Paris, France.

Corresponding author: M.-A. Harel, Laboratoire des Sciences du Climat et de l'Environnement, CEA-CNRS-UVSQ, Orme des Merisiers, Gif-sur-Yvette, FR-91191 Paris CEDEX, France. (mharel@lscce.ipsl.fr)

©2013. American Geophysical Union. All Rights Reserved.
0043-1397/13/10.1002/2013WR013596

some of the rainfall water is stored in microdepressions. As the rainfall rate increases, this stored water may either be released and routed downslope to other micropools, where it may infiltrate (or be stored again), or it may reach the plot outlet and produce measurable runoff [Darboux *et al.*, 2002a, 2002b]. Therefore, infiltration variability and microtopography, two properties that may be spatially correlated, give rise to the runoff-runon process. That is, runoff generated on an area with low infiltration capacity flows downslope and may infiltrate in another area with higher infiltration capacity [Hawkins and Cundy, 1987; Saghafian *et al.*, 1995; Corradini *et al.*, 1998].

[5] Lafforgue [1977] was one of the first authors to conduct a theoretical investigation of the role of this infiltration variability on runoff. Based on field observations in West Africa, he proposed to model the plot as a statistical ensemble of point infiltration capacities that are constant in time and described by either a uniform or a bimodal law. Using this approach, he showed how the average infiltration capacity for a plot increases with the rainfall rate. Hawkins and Cundy [1987] proposed the same statistical approach assuming that the domain, hillslope, or watershed, could be viewed as a set of parallel strips aligned along the slope with time-constant infiltration capacities distributed at random according to an exponential distribution. They also showed that the spatially averaged infiltration rate increases with rainfall rate and that it tends to a maximum value equal to the averaged infiltration capacity (called the maximum infiltration rate). Subsequently, Yu *et al.* [1997], Van Dijk and Bruijnzeel [2004], Stone *et al.* [2008], and Patin *et al.* [2012] successfully applied the “parallel strips” model to interpret runoff production experiments on plots of different dimensions, under both simulated and natural rainfall with varying types of land-cover and climate. The opposite arrangement, where the strips are orthogonal to the slope, has never been investigated theoretically until Jones *et al.* [2009]. It should be noted that the runoff-runon process can exist in this system but cannot exist in the parallel strips model.

[6] At larger scales, hillslopes and catchments also exhibit variability in their infiltration capacity. Vegetation, topography, and soil surface properties (natural or anthropogenic) are recognized to be important sources of variability [Dunne *et al.*, 1991]. Runon, which reduces the total runoff volume and sediment yield, is a hydrological process which must be taken into account in models [Saghafian *et al.*, 1995; Woolhiser *et al.*, 1996; Howes and Abrahams, 2003; Adams *et al.*, 2012]. Because of runon, the runoff volume at the stream is less than the sum of the volumes produced by each pixel of the hillslope or catchment.

[7] Several authors have suggested that the observed scale dependency of hillslope runoff (i.e., decrease of the runoff coefficient with domain size) is controlled by spatial and temporal variability in infiltration and, thus, by the runoff-runon process [Wood *et al.*, 1988; Cerdan *et al.*, 2004; Gomi *et al.*, 2008]. Others invoke the spatiotemporal variability in the rainfall rate [Wainwright and Parsons, 2002], vegetation [Lesschen *et al.*, 2009], topography or a combination of these [Wood *et al.*, 1988]. In association with the scaling of runoff volume, a rainfall intensity threshold has been observed for runoff generation. The threshold increases with the size of the domain [Cammere *et al.*, 2004; Hopp and McDonnell, 2009].

[8] One direct consequence of the runoff-runon process is that runoff does not take place homogeneously on the slope, but rather forms a network of partially connected runoff patterns. The recent concept of connectivity appears to be a promising framework for describing this organization and its evolution with rainfall [Bracken and Croke, 2007; Hopp and McDonnell, 2009]. Connectivity is used to describe the coalescence of runoff patterns during a rainfall event. This mechanism is important because it explains the rising limb of a hydrograph, as the patterns connect to the stream [Gomi *et al.*, 2008]. It is also helpful in explaining the scale effect and the rainfall intensity threshold mentioned previously [Hopp and McDonnell, 2009]. Although connectivity is now recognized as a determinant and possibly unifying concept in catchment hydrology [Western *et al.*, 2001], its interpretation and application is still ambiguous and requires a better and broader agreement among hydrologists [Michaelides and Chappell, 2009]. According to the connectivity concepts commonly used in the literature, connectivity can be either structural or functional [Antoine *et al.*, 2009]. Structural connectivity relates to the continuum properties of state variables such as soil characteristics and altitude, whereas functional connectivity is process-based and depicts the capacity of water to move in the system in response to a boundary stimulus [Antoine *et al.*, 2009; Wainwright *et al.*, 2011]. In our case, the state variable is the runoff-generating areas, hereafter referred to as rainfall excess areas, and the functional connectivity depicts the runoff-contributing areas (wet areas) [Sen *et al.*, 2010]. The central question resulting from these definitions is how to predict the connectivity of wet areas, given the connectivity of rainfall excess areas.

[9] Some recent research illustrates this runoff connectivity issue. Mueller *et al.* [2007] studied the connectivities of different hydrologic features in a semiarid shrubland environment and revealed their role in runoff connectivity. They showed that an appropriate representation of these connectivities in a distributed runoff model enables it to simulate realistic flow patterns and hydrographs. Based on runoff experiments performed on steep forest hillslopes, Gomi *et al.* [2008] discussed the relationships among scale effect, connectivity, land-cover, and rainfall. Sen *et al.* [2010] delineated spatially and temporally variable runoff-generation areas in an instrumented pasture hillslope. That study demonstrated that the connectivity of these areas and runon both have important impacts on the discharge hydrograph.

[10] The modeling approaches developed to study runoff generation on heterogeneous soils and to quantify the impact of runon on runoff volume and rate all rely on semi-analytical modeling and/or numerical simulation. The principal aim of these studies is to estimate the areal-average infiltration rate and consequently the runoff discharge at the outlet of the domain (plot, hillslope, or catchment). In semianalytical models, it is generally assumed that infiltration is Hortonian at the pixel scale and that the permeability at saturation is distributed spatially with a correlated log-normal distribution. These models ignore the runon process or take it into account empirically. For instance, Wood *et al.* [1986] neglect runon, and, assuming that the infiltration rate is given by Philip's equation, they propose expressions for the mean and variance of the infiltration rate (in

which the statistical mean is equal to the areal spatial mean if the domain is large enough). The impacts of variable rainfall rates and topography are also discussed by these authors. *Govindaraju et al.* [2006] propose a similar approach but with an infiltration rate given by the Green-Ampt model. They developed a semianalytical formulation for the expected areal-average infiltration. *Corradini et al.* [1998] and *Govindaraju et al.* [2006] performed some Monte-Carlo simulations of runoff on lognormal correlated hydraulic conductivity fields. They evaluated the impact of runoff on the mean and variance of hydrographs. *Morbidelli et al.* [2006, 2007] proposed to complete the model of mean infiltration rate developed by *Govindaraju et al.* [2006] with an empirical term representing runoff. They also showed that this mean effective infiltration rate can be incorporated into a kinematic wave equation to simulate the initial runoff-runon by an equivalent runoff process. Finally, *Nahar et al.* [2004] and *Michaelides and Wilson* [2007] further extended the work of *Corradini et al.* [1998] to analyze the effect of runoff at the hillslope scale. They studied the influence of the hydraulic conductivity parameters (mean, variation coefficient, correlation length, as well as nugget effects) on the mean infiltration and the hydrograph in relation to the rainfall rate. All of these developments have been validated with Monte-Carlo simulations.

[11] These theoretical modeling approaches have not addressed the physics of runoff-runon at an intermediate scale between the pixel and the domain. Yet this is the relevant scale to describe runoff generation, its spatial organization into patterns, and the role played by runoff. The spatial organization of runoff is a key process in the runoff connectivity, which depends directly on the infiltration capacity heterogeneity and connectivity. We propose to quantitatively address these issues for the permanent rainfall case. Our work combines an original idea presented by *Jones et al.* [2009] in a conference paper with the work done by *Allard et al.* [1993] on the connectivity of lithofacies in petroleum geostatistics.

[12] Assuming that infiltration capacities do not evolve with time, *Jones et al.* [2009] showed that the equation governing the runoff-runon process along a flat 1-D slope is identical to the equation governing the waiting time of a customer in a single server queue. Queueing theory, which is usually applied in telecommunications, computing, and traffic management, is a consequential branch in stochastic processes [*Asmussen*, 2003]. It describes the waiting time of customers arriving randomly at one or several serving desks to receive a service of random duration. On the basis of this mathematical equivalence, *Jones et al.* [2009] used the vast literature on queueing processes to propose expressions for the mean and variance of the runoff flow rate and for the connected length contributing to the flow at the outlet. This work describes a system, plot, or hillslope, conceptualized as a series of homogeneous parallel strips orthogonal to the slope.

[13] In addition, *Allard et al.* [1993] showed how to construct a random field of a given correlation structure that is conditioned by connectivity constraints. For this purpose, they introduced the connectivity function (also defined in *Stauffer and Aharony* [1994]) as the probability that two points are connected by a continuous path in the simulated lithofacies. This multipoint statistics framework allows the

characterization of structures that classical statistics cannot assess through correlation functions. *Western et al.* [2001] and *Michaelides and Chappell* [2009] recommended the use of the geostatistical connectivity as a framework for quantifying hydrological connectivity.

[14] In this paper, we study the runoff generation and spatial organization on a flat 1-D slope during a rainfall event with steady and uniform intensity. Microtopography and, therefore, runoff storage in microdepressions are neglected. Infiltration excess overland flow is the only mechanism assumed to produce runoff, and the saturation excess mechanism (Dunne runoff) is disregarded.

[15] Local infiltration is described by a threshold infiltration function that depends on a single parameter called soil infiltrability. Infiltrability is a time-constant infiltration capacity that encompasses all physical processes influencing infiltration locally, such as crusting, vegetation, or soil structure [*Patin et al.*, 2012]. As previously discussed, this homogenized approach is classically used in the study of runoff production on plots under simulated or natural rainfall. The ponding-time is neglected. All of the available water (runon plus rainfall) infiltrates instantly as long as the water supply is inferior to infiltrability [*Hawkins and Cundy*, 1987; *Yu et al.*, 1997; *Van Dijk and Bruijnzeel*, 2004; *Patin et al.*, 2012]. In long-term rainfall simulation experiments, for instance, this assumption is justified when the infiltration rate has reached steady state. This is the nominal experimental situation to which our model applies, supposing that the system does not evolve with time. When the soil is homogeneous from the top to the bulk, infiltrability is the soil saturated conductivity. We note that this definition of infiltrability is different of that proposed by *Hillel* [1998].

[16] Four uncorrelated distributions of infiltrability, representative of soil heterogeneities in a catchment, are considered: exponential, bimodal, lognormal, and uniform. In the lognormal case, the effects of correlation and nuggets are also studied. The exponential distribution has been used by many authors, and applied from the plot to the watershed scale. *Hawkins and Cundy* [1987] were the first authors to propose this distribution. They showed that it reproduced the observed steady state infiltration rates of simulated rainfall experiments very well. *Yu et al.* [1997] and *Paige et al.* [2002] then successfully adopted this distribution for small-scale domains. It should be noted that the choice of this distribution was motivated by mathematical reasons (it is a one-parameter distribution and is easily integrated) rather than experimental observations. The choice of a bimodal distribution is motivated by observations and measurements of runoff produced on crusted soils and in semiarid areas. The infiltration capacity of a crusted soil is very low and depends on the type of crust [*Casenave and Valentin*, 1992; *Le Bissonnais et al.*, 2005]. Crusted soils may develop natural cracks or microsteps where water can easily infiltrate [*Esteves and Lapetite*, 2003]. In certain semiarid areas of West Africa, vegetation patterns consisting of alternating areas of vegetation and bare soil covered by crusts are frequently observed. The vegetation patches are preferential zones of infiltration [*Bromley et al.*, 1997].

[17] The lognormal distribution is usually employed to describe the spatial variability of the saturated hydraulic conductivity at the hillslope scale [e.g., *Nielsen et al.*,

1974; Russo and Bresler, 1981]. The uniform distribution is considered as the standard reference distribution when nothing can be said of the histogram of a measured variable [Lafforgue, 1977].

[18] The objective of this study is to understand, for each distribution and as a function of the rainfall rate, how: (1) the one-point statistics (pdf, mean, and variance) of infiltrability and runoff flow rate are related, (2) the runoff patterns (number, length, and density) and the connectivity of the wet areas are related to those of the rainfall excess patterns and area, and (3) the presence of a zero flow upslope boundary condition affects runoff statistics and the runoff coefficient (an indicator of a scale effect).

[19] Theoretical developments based on queuing theory and numerical simulations are used to address these tree points. The runoff flow rate statistics are only known precisely for the exponential infiltrability distribution [Asmussen, 2003]. Bimodal, lognormal, and uniform distributions are not common in queuing theory and, to the authors' knowledge, no exact theoretical results have been published on them. We here propose some results on the bimodal. The mathematical properties of the runoff flow rate probability density function, which is under studied in queuing theory as well, is discussed in detail. Finally, the connectivity of the runoff flow rate has never been addressed theoretically.

[20] This article is organized in two main sections. The first briefly describes the physics of the system and its analogy to a queuing process. We also present a short recapitulation of the queuing variables of interest with their available theoretical expressions. The simulation results addressing the three questions identified above are presented and discussed in the second section

2. Theoretical Model: Runoff-Runon as a Queuing Process

2.1. Runoff-Runon Model

[21] The domain, which may represent either a plot or a hillslope, is modeled as a simple idealized one-dimensional flat soil surface. It is divided into N pixels of size Δx (L). The infiltrability I ($[LT^{-1}]$) is distributed randomly and assumed to be constant in time. The rainfall rate R ($[LT^{-1}]$) is a constant in both space and time.

[22] Let us call Q_i the runoff flow rate per unit length from pixel i to pixel $i+1$ ($[L^2T^{-1}]$), where index i increases downslope (Figure 1). At steady state, the runoff mass balance in pixel i reads

$$\frac{Q_i}{\Delta x} = \left(\frac{Q_{i-1}}{\Delta x} + R_i - I_i \right)^+ \quad (1)$$

where R_i and I_i are the rainfall and infiltration rates in pixel i , respectively ($[LT^{-1}]$) and A^+ stands for $\max(A, 0)$. All the simplifying assumptions and justifications associated with this formulation of runoff-runon are developed in the introduction. If $Q_{i-1} = 0$ (no runon), runoff is produced in pixel i providing that $R_i > I_i$. Otherwise, the condition $(Q_{i-1}/\Delta x + R_i) > I_i$ is required to obtain $Q_i > 0$. The total water flow rate $Q_{i-1}/\Delta x + R_i$ can be considered as an equivalent rainfall rate for pixel i . The boundary condition in pixel

$i = 1$ is an imposed runoff flow rate Q_0 . Hereafter, we choose $\Delta x = 1$, write $Q_i \equiv Q_i/\Delta x$ and still call Q_i the runoff flow rate, though it has a velocity dimension ($[LT^{-1}]$).

[23] Simulations show that, for a realization of a given random field of infiltrability, the random runoff flow rate defines wet ($Q \neq 0$) and dry ($Q = 0$) areas of random positions and extensions in the domain. We need to distinguish these wet areas from the zones where runoff would be produced in absence of runon, that is, where $R_i > I_i$. Such areas are therefore called *rainfall excess areas*. Similarly, we call the zones where $R_i < I_i$ *rainfall deficit areas*. It is worth noting that the rainfall excess areas are included in the wet areas.

2.2. Queuing Processes

[24] In this section, we provide a short description of queuing theory and a review of the basic results for some queues of interest in hydrology.

[25] Queuing theory describes the waiting time of customers arriving randomly at one or several serving desks to receive a service of random duration. A queuing system is characterized by the number of servers, the distributions of customer arrivals and service times, and eventually the size of the room (finite buffer) and the queuing discipline [Asmussen, 2003]. We focus here on first-in first-out (FIFO) single server queues with constant service time, random interarrival time, and infinite room.

[26] This type of queue describes the following sequence: if a customer i arrives at time t_i when the server is free, he is immediately served with a service time S_i . After that period he leaves the system. If the next customer $i+1$ arrives (at t_{i+1}) when the server is still engaged with customer i , he waits in the queue during a waiting time $W_{i+1} = S_i - (t_{i+1} - t_i)$ until he is served with a service time S_{i+1} . $T_i = t_{i+1} - t_i$ is called the interarrival time. If $T_i \geq S_i$, customer $i+1$ is served immediately, his waiting time is null, and the queuing process restarts. More generally, if a customer arrives when the server is busy, he waits in a queue until his predecessors have been served. The waiting time of customer i is given by the following relationship [Asmussen, 2003]:

$$W_i = (W_{i-1} + S_i - T_i)^+ \quad (2)$$

[27] The (nonintuitive) correspondence between the 1-D hydrological variables (equation (1)) and the queue parameters was established by Jones *et al.* [2009] as follows: pixel i is the customer's number, infiltrability I_i is the interarrival time T_i between customers i and $i+1$, the rainfall rate R_i is the service time S_i of customer i , and Q_i is the waiting time W_i of customer i , i.e., the time spent in the queue between arrival and beginning of service (Figure 2).

[28] In the early works on queues, most authors assumed that each of the variables, interarrival times, and service times, were uncorrelated (two successive arrival or service times are independent) and that the two variables were independent [Asmussen, 2003]. Later on, these two assumptions were relaxed and the impact of correlated arrivals, or correlated arrival and service [Adan and Kulkarni, 2003], were investigated. In the following presentation, we adopt the original assumptions.

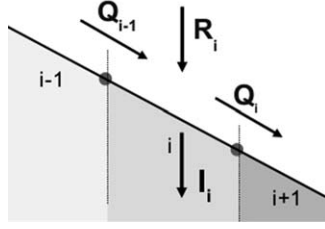


Figure 1. 1-D slope at pixels $i-1$, i , and $i+1$. Mass balance at pixel i with runoff Q , rainfall intensity R and infiltrability I .

[29] Kendall [1951] introduced an $A/B/n$ notation to characterize the queuing models. The first letter specifies the interarrival time distribution, the second specifies the service time distribution, and n is the number of servers. For example, the letter G is used for a general distribution, M for the exponential distribution (M stands for Memoryless and represents a Poisson process) and D for deterministic times.

[30] The basic quantity describing the runoff statistics is the distribution function of the runoff flow rate $F_i(x) = \Pr(Q_i \leq x)$, where $\Pr(A)$ denotes the probability of an event A and $F_i(x)$ is defined for $x \geq 0$. Lindley [1952] showed that, at distances far from the boundary condition (pixel $i = 0$), the distribution becomes independent of i and obeys the integral equation:

$$F(x) = \int_{y \geq 0} F(y)g(x-y)dy \quad (3)$$

where $g(x)$ is the probability density function of $R - I$. It is interesting to observe that the runoff flow rate distribution does not depend on the respective distributions of R and I but only on the distribution of their difference.

[31] Lindley [1952] showed that this integral has a finite solution when $\langle R \rangle < \langle I \rangle$, where $\langle X \rangle$ is mean X . In this case, $F(x)$ describes an equilibrium distribution of runoff flow rates. In queuing theory the parameter ρ (dimensionless), defined as the ratio between mean service time and mean interarrival time, is of primary importance. It measures the traffic as well as the stability of the queue. In hydrology, $\rho = \langle R \rangle / \langle I \rangle$ stands for the dimensionless rainfall intensity. If $\rho < 1$, the mean runoff flow rate is constant if observed sufficiently far from the upslope boundary condition (steady state). Otherwise, when $\rho > 1$, Q_i increases monotonously with i , and the entire slope is flooded. In this case, $Q_n \rightarrow n(\langle R \rangle - \langle I \rangle)$ when $n \rightarrow \infty$. The critical case $\rho = 1$ defines the state of the system for which it is certain that a dry pixel can appear but the probability of this occurrence tends to zero [Lindley, 1952].

[32] Several authors noted that $\rho = 1$ is a critical value in the Monte-Carlo simulation of hillslopes or catchments [Saghafian et al., 1995; Nahar et al., 2004; Morbidelli et al., 2006; Jones et al., 2009]. The case of a periodic variation of infiltrability best illustrates the transition at $\rho = 1$. Indeed, if $\langle I \rangle$ is the mean infiltrability for a period, it is clear that when $\rho < 1$, wet areas develop periodically and when $\rho > 1$, runoff floods the system.

[33] This transition is also well established in percolation theory. Percolation is clearly related to our system, as will be demonstrated further on. The 1-D system, the only one

for which exact results are available in this framework, percolates when all the pixels on a slope are wet ($Q > 0$). Thus, the percolation threshold, defined as the proportion of wet pixels (ρ) at which a wet pattern connects the upper and lower boundaries of an infinite slope, is one. Further explanations of the links between percolation and connectivity are developed in section 2.3 and in the paper by Renard and Allard [2011].

[34] The integral equation (3) is not easy to solve. The classical way is to use the Wiener-Hopf method [Smith, 1953]. There are only a few cases where the solution of equation (3) is known [Asmussen, 2003]. The two most important ones with respect to our hydrological problem are where: (i) the infiltrability and rainfall probability density functions (pdf) are negative exponential ($M/M/1$ queue); (ii) the infiltrability pdf is negative exponential and rainfall rate pdf is a Dirac centered on a deterministic value (constant rainfall rate, $M/D/1$ queue). Other queues have been investigated, mainly in the domain of communication systems, but in the general case $G/G/1$, equation (3) needs to be solved numerically [Konheim, 1975].

[35] Here we focus on the $M/D/1$ system, which corresponds to our hydrological settings, even though the $M/M/1$ queue is the most studied because of the mathematical properties of the exponential function [e.g., Asmussen, 2003]. All of the following theoretical results have been obtained under the stationary assumption ($\rho < 1$) unless stated otherwise.

[36] For $M/D/1$, the cumulative distribution function is a step function expressed as [Erlang, 1909]:

$$F(x) = (1-\rho) \sum_{k=0}^m \frac{[-\lambda(x-kR)]^k}{k!} \exp[\lambda(x-kR)] \quad (4)$$

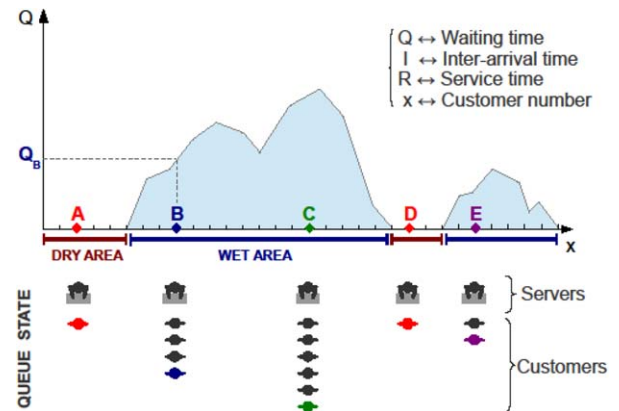


Figure 2. Queuing theory and 1-D connectivity concepts. Q is runoff, I is infiltrability and R is rainfall rate. x is the number of pixels as well as the number of customers having entered the room since system initialization ($x = 0$), or customer number. At point A (or D): no waiting time ($Q = 0$), but the server is not idle. In dry areas, all customers are served immediately. At point B: the last customer to enter the room waits Q_B before being served. Linking the waiting time with the number of customers in the queue is not trivial. The points (B, C) are connected, the points (A, B) and (C, E) are not.

where $mR \leq x < (m+1)R$, R is the constant rainfall rate, $\langle I \rangle = 1/\lambda$ is the mean infiltrability and $\rho = R\lambda$.

[37] The one-point statistical moments of the runoff flow rate can be deduced from the distribution function $F(x)$. The mean runoff flow rate for the queue $M/G/1$, which encompasses both the $M/M/1$ and $M/D/1$ queues, is given by the well-known Pollaczek-Khintchine formula [Asmussen, 2003]:

$$\langle Q \rangle = \frac{\lambda \langle R^2 \rangle}{2(1-\rho)} \quad (5)$$

[38] The second moment is [Iliadis and Fuhrmann, 1992]:

$$\langle Q^2 \rangle = \frac{\lambda \langle R^3 \rangle}{3(1-\rho)} + \frac{\lambda^2 \langle R^2 \rangle^2}{2(1-\rho)^2} \quad (6)$$

where $\langle R \rangle$ and $\langle R^2 \rangle$ are the first and second moments of the rainfall rate distribution ($\langle R \rangle = R$ and $\langle R^2 \rangle = R^2$ for $M/D/1$).

[39] Jones et al. [2009] propose to use the approximate expressions of $\langle Q \rangle$ and $\langle Q^2 \rangle$ as derived heuristically by Kramer and Langenbach-Belz [1976] and Bhat [1993] for many (if not all) rainfall and infiltrability distributions. These approximations are based on a two-moment description of the distributions. Therefore infiltrability distributions which have the same mean and variance, as in our case, cannot be distinguished.

[40] The two point statistics (covariance) of Q have rarely been considered in queuing theory [Daley, 1968]. It is crucial to observe that whereas the infiltrabilities of two neighboring pixels are not correlated, the runoff flow rates on these pixels are. A review of the results on two-point statistics of different quantities in queuing theory can be found in Reynolds [1975].

[41] Most of queuing theory has been developed with the assumption that interarrival times (i.e., infiltrability) are not autocorrelated. To our knowledge, Tin [1985] was the first author to take correlation into account. He considered the case where rainfall is an uncorrelated exponential and infiltrability (T_i) follows a first-order Markov process: T_{i+1} is only correlated with T_i and the conditional density function is the Downton's bivariate exponential distribution [Hunter, 2007]:

$$f(T_{i+1}|T_i) = \frac{\lambda^2}{1-\kappa} \exp\left(\frac{-\lambda(T_i+T_{i+1})}{1-\kappa}\right) I_0\left(\frac{2\lambda\sqrt{\kappa T_i T_{i+1}}}{1-\kappa}\right) \quad (7)$$

where κ is the correlation coefficient between T_i and T_{i+1} ($0 \leq \kappa < 1$), $1/\lambda$ is the mean arrival time and I_0 is the Bessel function of the first kind of the zeroth order. The marginal distribution function of each T_i is exponential. In the uncorrelated case $\kappa = 0$, then the correlation increases with κ . The physical signification of this coefficient may be found in Lampard [1968]. Tin gives various results, among them the runoff distribution. We will use Tin's results in section 3.4 exclusively, because the rest of our developments are based on the assumption that infiltrability is not correlated.

[42] For any queue $M/G/1$, the dimensionless rainfall rate ρ is the probability that $Q \neq 0$ (respectively, $1 - \rho$ the probability that $Q = 0$). This parameter describes the per-

centage of the domain where runoff occurs, called the wet area fraction and denoted ω (the percentage of the domain area with no runoff is called dry area fraction and denoted $\bar{\omega} = 1 - \omega$). For queues other than $M/G/1$, the wet area fraction varies nonlinearly with ρ , as we shall see in section 3.2. It is defined as:

$$\omega = 1 - F(Q=0) \quad (8)$$

[43] As long as $\rho < 1$, runoff is organized along the slope as a succession of wet and dry zones of random positions and extensions. These areas correspond to the busy and idle periods of the server, as previously observed by Jones et al. [2009]. The number n of pixels of a given wet zone corresponds to the $n + 1$ customers served during a busy period. This difference accounts for the fact that the first person served at the beginning of a busy period does not wait and, therefore, does not relate to a wet pixel (see Figure 2). The distribution of the number of customers served during a busy period is equivalent to the distribution of wet zone lengths. This distribution, called $P(n, \rho)$ where $n = 1, 2, \dots$ is the number of wet pixels, is central to the definition of the wet area connectivity. Clearly we may write:

$$P(n, \rho) = F(0) \Pr(X_1 < Y_1, X_2 < Y_2, \dots, X_n > Y_n) \quad (9)$$

where $X_k = I_1 + \dots + I_k$ and $Y_k = R_1 + \dots + R_k$. Prabhu [1960] finds that for the $M/D/1$ queue:

$$P(n, \rho) = (1-\rho)\rho^n e^{-(n+1)\rho} \frac{(n+1)^n}{(n+1)!} \quad (10)$$

[44] This expression is defined in the ensemble of infiltrability realizations, whereas Prabhu considers the ensemble of busy periods, i.e., the ensemble of wet zones. This is why the factor $1 - \rho$ appears in our expressions.

[45] Two interesting quantities may be derived from the preceding distribution: the mean number of wet zones per unit length, and the mean length of a wet zone. The length of a wet zone is equal to the number of customers served during a busy period minus one, as explained above. Therefore, the distributions of Prabhu must be reformulated in the ensemble of wet areas. After correction, the mean length $M/D/1$ is:

$$\langle l \rangle = \frac{\rho}{1-e^{-\rho}} \frac{1}{1-\rho} \quad (11)$$

where the mean number of customers for $M/G/1$ is $1/(1-\rho)$ [Asmussen, 2003]. The mean number of wet zones per unit length $\langle N \rangle$ is the sum over n of the probability $P(n, \rho)$ (equation (10)). For $M/D/1$:

$$\langle N \rangle = (1-\rho)(1-e^{-\rho}) \quad (12)$$

[46] When $\rho \rightarrow 1$, the moments of Q (equations (5) and (6)) become infinite and $\langle N \rangle$ tends to zero: runoff takes place over the whole domain and there is a single wet zone of infinite length. As long as $\rho < 1$, the spatial organization of wet zones can be described as a renewal process [Feller, 2008]. This class of stochastic processes is used to model

the independent, identically distributed occurrences at which the process restarts itself. Each wet pixel located downslope of a dry pixel represents a regeneration point that is governed by a Poisson process [Van Leeuwaarden *et al.*, 2010]. Therefore, the succession of wet zones along the domain is the aggregation of independent, identically distributed blocks of random length [Asmussen, 2003]. The independence of wet areas also indicates that the spatial correlation between two wet pixels located in separate wet zones is null. In other words, the information transferred by runoff cannot spread beyond a given wet zone, and the runoff process regenerates itself at an occurrence independently of the past. Powerful asymptotic results are obtained thanks to this property [Stidham, 1972; Van Leeuwaarden *et al.*, 2010], which will be further discussed in section 3.5.

[47] As previously stated, analytical results are only known for the exponential infiltrability distribution. In Appendix A, we develop some partial results for the bimodal distribution, which we call $2D/D/1$, where I_i may be equal to I_A , with probability α , or I_B , with probability β ($\alpha + \beta = 1$). The outputs are the mean and variance of the runoff flow rate, as well as the wet area fraction. We show that they all depend on the root of equation $z = ((1 - \beta) + \beta z)^N$. The results are obtained for discrete values ρ ($\rho = 1/N$ where N is any integer satisfying $\rho < \beta$) and are extrapolated to the continuous case where ρ varies between 0 and β . The extrapolation means that N is replaced by $1/\rho$.

2.3. Connectivity

[48] As discussed in section 1, functional connectivity needs to be distinguished from structural connectivity. In our problem, structural connectivity relates to the connectivity of rainfall excess areas ($R > I$), whereas functional connectivity is applied to wet areas ($Q \neq 0$). Nevertheless, we assume that both connectivities, in their application to runoff or infiltrability, can be quantified by a unique parameter.

[49] Knudby and Carrera [2005] compared nine indicators of connectivity and found that to link the structural and functional connectivities, one should consider directional multiple-point statistics applied to binary data such as the connectivity function. This indicator, first introduced by Allard *et al.* [1993] in a geological context, has been successfully used by Western *et al.* [2001], Grayson *et al.* [2002], and Antoine *et al.* [2009] in surface hydrology.

[50] The connectivity function applies to the indicator Z , which is a binary transform obtained by thresholding the original data. If structural connectivity is considered, the infiltrability data are thresholded by rainfall intensity, consequently $Z_i = 1$ for $R_i > I_i$ and $Z_i = 0$ otherwise. To assess the functional connectivity, we define $Z_i = 1$ when runoff is observed at pixel i ($Q_i \neq 0$) and $Z_i = 0$ otherwise ($Q_i = 0$). Two pixels i and $i + n$ are said to be connected if they belong to the same pattern, that is, the same series of 1 (points B and C in Figure 2). The connectivity function $\tau(h, \rho)$ is the probability that two pixels separated by the distance $h\Delta x$ are connected for a given rainfall rate ρ [Allard *et al.*, 1993; Western *et al.*, 2001]. It equals unity when there is a continuous path of length h connecting any pair of pixels in the domain. If we call $\tau_I(h, \rho)$ and $\tau_Q(h, \rho)$ the structural and functional connectivities, respectively, the runoff-runon process leads to the inequality $\tau_I(h, \rho) < \tau_Q(h, \rho)$.

[51] The connectivity integral scale $L_{\tau_z}(\alpha = I, Q)$ is defined as [e.g., Western *et al.*, 2001]:

$$L_{\tau_z}(\rho) = \int_0^\infty \tau_z(h, \rho) dh \quad (13)$$

[52] The functional connectivity integral scale L_{τ_Q} represents the average distance over which pixels are connected. L_{τ_Q} increases with the rainfall rate ρ and the degree of connectivity in the domain. Western *et al.* [2001] explain the differences among bivariate indicator methods (vario-grams), the connectivity function and its integral.

[53] In a single infinite realization of infiltrability, the connectivity function, whether structural or functional, is evaluated as the ratio between the number of pairs of pixels separated by h and belonging to the same $Z = 1$ pattern (connected pairs, such as (B, C) in Figure 2), and the number of pairs of two $Z = 1$ pixels that are h apart (wet pairs, connected or not, such as (B, C) and (C, E) in Figure 2) [Allard *et al.*, 1993]. It is easy to show that:

$$\tau_z(h, \rho) = \frac{\sum_{k=1}^\infty k P_z(h+k, \rho)}{C_z(h, \rho)} \quad (14)$$

where $C_z(h, \rho)$ is the covariance of the $Z = 1$ distribution. For infiltrability, the covariance is $C_I(h, \rho) = (P^-)^2 + [(P^-) - (P^-)^2]\delta(h)$, with $\delta(h)$ as the Dirac function. The structural connectivity is simply written:

$$\tau_I(h, \rho) = \frac{(P^-)^{h+1}}{(P^-)^2 + [(P^-) - (P^-)^2]\delta(h)} \quad (15)$$

[54] This expression is valid for any h , positive or null. It can be simplified when $h \geq 1$ as

$$\tau_I(h, \rho) = (P^-)^{h-1} \quad (16)$$

[55] The connectivity integral scale (equation (13)) is simply $L_{\tau_I}(\rho) = 1/P^+$. It should be noted that two $Z = 1$ patterns distant of Δx are always connected. $Z = 1$ patterns must be at least separated by $2\Delta x$ to be differentiated. This is why $\tau_I(0, \rho) = \tau_I(1, \rho) = 1$. The functional connectivity $\tau_Q(h, \rho)$ has no explicit expression to our knowledge. If we assume that runoff is independently distributed in each pixel with a probability ρ , then

$$\tau_Q(h, \rho) \approx \rho^{h-1} \quad (17)$$

[56] In their review on connectivity for subsurface flow and transport, Renard and Allard [2011] recall a fundamental result in percolation theory: the connectivity function may be approximated by an exponential for large distances h according to the following equation (which is valid far from the percolation threshold):

$$\tau(h) = \exp(-h/L_\tau) \quad (18)$$

[57] This equation is exact for the 1-D structural connectivity function [Stauffer and Aharony, 1994]. Renard and Allard [2011] assert that an excellent approximation of the connectivity integral scale is given by the product:

$$L_\tau \simeq n_p(p) \quad (19)$$

where n_p is the number of permeable cells for a given proportion p (i.e., number of wet pixels for a given rainfall rate ρ) and (p) is the proportion of connected pairs in the permeable phase among all the pairs of permeable cells (i.e., proportion of connected wet pixels among all the pairs of wet pixels). From equation (19), one can see that:

$$L_{\tau_Q} \simeq \frac{\langle l_Q^2 \rangle}{\langle l_Q \rangle} \quad (20)$$

where $\langle l_Q \rangle$ is the mean length of a wet zone (equation (11)) and $\langle l_Q^2 \rangle$ is the second-order moment of l_Q . It can be calculated with *Prabhu's* pdf $P(n, \rho)$ (equation (10)), for $M/D/1$:

$$\langle l_Q^2 \rangle = \frac{1}{1-e^{-\rho}} \left(\frac{1}{(1-\rho)^3} - \frac{2}{1-\rho} + 1 \right) \quad (21)$$

[58] We believe that equation (19) has been derived for a slightly different definition of the connectivity function (denoted $\tau^*(h, \rho)$) than the one used in the present paper. *Renard and Allard* [2011] refer to *Stauffer and Aharony* [1994], where the connectivity function is defined as the ratio between connected pairs and the pairs of pixels for which at least one of them belongs to the permeable phase. The connectivity function we previously defined has the same numerator but a more restricted (smaller) denominator: both pixels of the pair must belong to the permeable phase. According to *Stauffer and Aharony* [1994]:

$$\tau_\alpha^*(h, \rho) = \frac{\sum_{k=1}^{\infty} k P_\alpha(h+k, \rho)}{\sum_{k=1}^{\infty} k P_\alpha(k, \rho)} \quad (22)$$

[59] As a consequence, the integral connectivity scale of *Renard and Allard* [2011] (equation (19)) should differ from (and exceed) ours, which is based on the definition of the connectivity function given by *Allard et al.* [1993], or by *Western et al.* [2001] (equation (14)).

[60] Although the connectivity function appears to be the best available indicator to describe overland flow connectivity, it is possible to further characterize the runoff organization along the slope by considering additional (but nonindependent) indicators. Among these, we consider quantities defined in the previous section to describe runoff patterns statistics: the wet area fraction ω (equation (8)), the wet zone lengths distribution $P(n, \rho)$ (equation (9)), the mean length of a wet zone $\langle l \rangle$ (equation (11)), and the mean number of wet zones per unit length $\langle N \rangle$ (equation (12)). $P(n, \rho)$ provides a typology of the runoff patterns, while ω relates to the degree of wetness over the surface. The sum of the pattern size distribution $P(n, \rho)$ over the length n gives the mean number of patterns $\langle N \rangle$ as a function of rainfall.

[61] The wet area fraction ω also relates to the near connectedness, whereas the connectivity function does not. This limitation of the connectivity function is linked to the choice of domain and mesh size made by the modeler. *Western et al.* [2001] noted that the apparent near connectedness is scale dependent, as are the connectivity measures.

[62] Below, we extend these definitions and notations to infiltrability. For the $Z = 1$ patterns, whether associated to Q or I , we define: $P_\alpha(n, \rho)$ the pattern length distribution, ω_α the area fraction (either wet or rainfall excess), $\langle l_\alpha \rangle$ the mean pattern length and $\langle N_\alpha \rangle$ the mean number of patterns per unit length, where $\alpha = I, Q$. If we call $P^- = Pr(I < R)$ and $P^+ = Pr(I > R)$ then we can easily find that $\omega_I = P^-$, $P_I(n, \rho) = (P^+)^2 (P^-)^n$ and $\langle N_I \rangle = (P^+) (P^-)$. These results are given in the ensemble of pixels, as opposed to the ensemble of patterns, for which results differ slightly (for instance, $P_I(n, \rho) = (P^+) (P^-)^n$ when patterns are considered). $\langle l_I \rangle = (P^+)^{-1}$ in the patterns set, the only relevant ensemble for this quantity. We have $P^+ = e^{-\rho}$ for $M/D/1$ [Asmussen, 2003], and $P^+ = \alpha$ for $2D/D/1$.

[63] An important property reflecting the runoff-runon process and one to bear in mind when analyzing the topology of the patterns distribution is:

$$\begin{cases} X_I(\rho) < X_Q(\rho) \\ X_Q(\rho) \rightarrow X_I(\rho), \quad \text{as } \rho \rightarrow 0 \end{cases} \quad (23)$$

where X stands for any of the variables defined in this section.

3. Simulation and Discussion

3.1. Numerical Simulation

[64] All of the simulations and the analyses of results were performed with *R* statistical software.

[65] We solve equation (1) on a flat 1-D slope of length $L = 14,000$ pixels, with $\Delta x = 1$. Each pixel is assigned a random value of infiltrability. These are generated according to an uncorrelated probability distribution, either lognormal, exponential, bimodal, or uniform.

[66] All the parameters are dimensionless. Such definitions are obtained by dividing the original parameter by the mean infiltrability, in the same way as ρ stands for the rainfall intensity. The lognormal, exponential, and bimodal distributions have the same mean infiltrability and standard deviation: $\langle I \rangle = 1$ and $\sigma_I = 1$. The uniform distribution is constant between $I_A = 0$ and $I_B = 2$ and also has the same mean but a slightly lower standard deviation: $\sigma_I = 1/\sqrt{3}$. Because I must be positive, it is not possible to impose both $\langle I \rangle = 1$ and $\sigma_I = 1$ for a uniform distribution. In the bimodal distribution, $\alpha = 0.5$ is the probability of mode $I_A = 0$ and $\beta = 1 - \alpha$ is that of mode $I_B = 2$. The rainfall intensity is constant in space and time. It may vary between zero and two times the mean infiltrability ($0 \leq \rho \leq 2$).

[67] The no-flow boundary condition in the first pixel influences the flow rate distribution over a certain distance. Simulations show that for rainfall values up to approximately $\rho = 0.9$, the 2000 first upslope pixels have to be removed from the simulations to avoid this influence. For $\rho > 0.9$, the distance becomes much larger and diverges as $\rho \rightarrow 1$ (see section 3.5, for a discussion on the impact of the boundary condition). Therefore, all the quantities describing the flow rate are computed by spatial averaging along the domain of length $L = 12,000$ pixels. In the following sections, the simulated and theoretical results obtained for $M/D/1$ and $2D/D/1$ are systematically compared whenever theoretical developments are available.

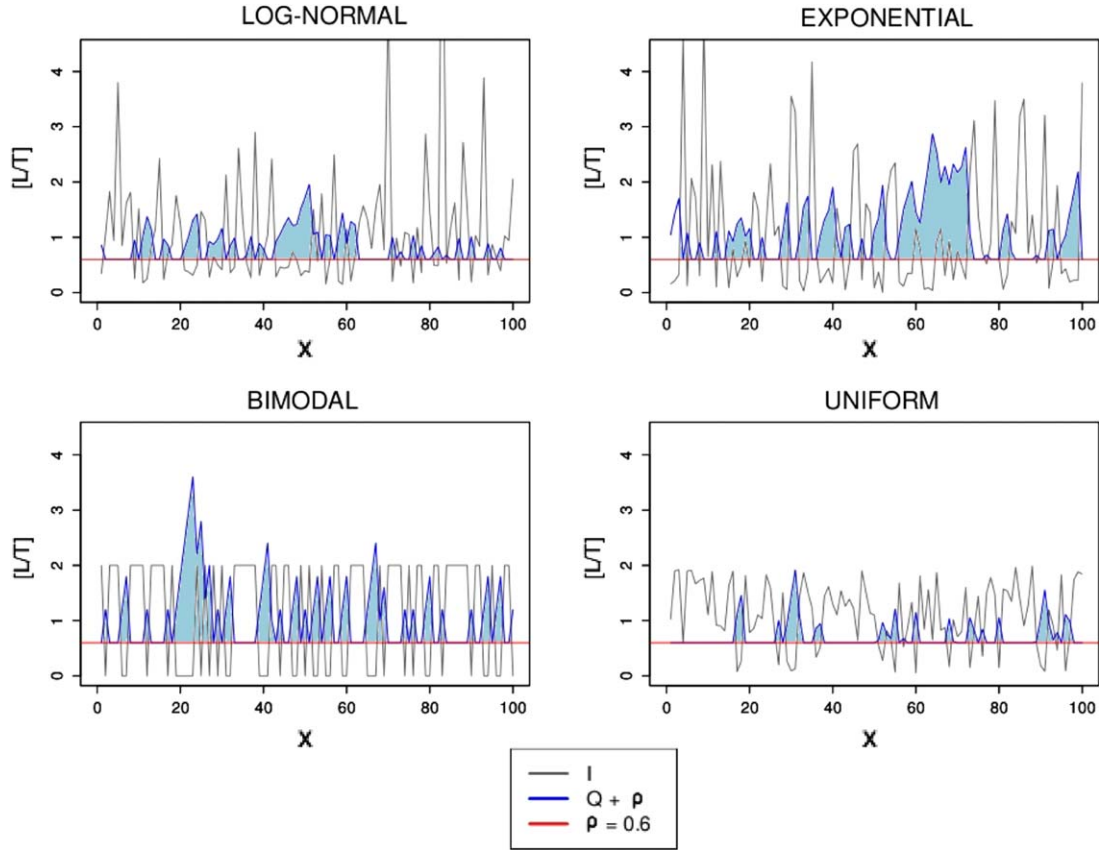


Figure 3. Spatial organization of runoff (Q) and infiltrability (I) for rainfall $\rho = 0.6$.

3.2. One-Point Statistics

[68] Figure 3 displays, for $\rho = 0.6$, the distribution of runoff along a portion of the domain for the four uncorrelated infiltrability distributions. It is clear that the spatial organization of runoff depends on the nature of the infiltrability law. The runoff-runon process occurs for every distribution: runoff arises in areas where $R > I_i$ and may propagate in immediate downstream zones where $R < I_i$. The highest runoff flow rate occurs for the bimodal distribution and the lowest for the uniform, while the exponential is the second highest after the bimodal. Neglecting runoff, i.e., for small values of ρ , the probability of runoff production $P^- = \Pr(I < R)$ at a pixel with no upstream inflow follows the observed hierarchy. Indeed, the distributions for which small I have high probabilities, such as the exponential, produce more runoff than other distributions. As a consequence, the rank of the bimodal law depends on the probability α of mode I_A . We can clearly see that all of the functions and parameters associated with $R - I$ are constant for $\rho < 1$ in the bimodal case.

[69] The mean runoff flow rate, $\langle Q \rangle$, is plotted as a function of ρ in Figure 4. Because the results concerning the variance σ_Q^2 are similar to those obtained for $\langle Q \rangle$, we did not include the associated curves. The following comments may apply to σ_Q^2 or to $\langle Q \rangle$ without distinction. The nonlinearity of runoff production with respect to rainfall intensity is obvious, especially for values of ρ between 0.5 and 1. Clearly the type of distribution has a great influence on

runoff production, whatever the value of ρ . The same hierarchy as is observed qualitatively in Figure 3 appears. The mean flow rate is multiplied by several orders of magnitude between bimodal and uniform: for instance $\langle Q_{BIM} \rangle \approx 3.5 \langle Q_{UNI} \rangle$ when $\rho = 0.6$.

[70] As a consequence of equation (23), the mean and the variance of Q tend to 0 in the same way as the mean and the variance of $R - I$ does when $\rho \rightarrow 0$. This

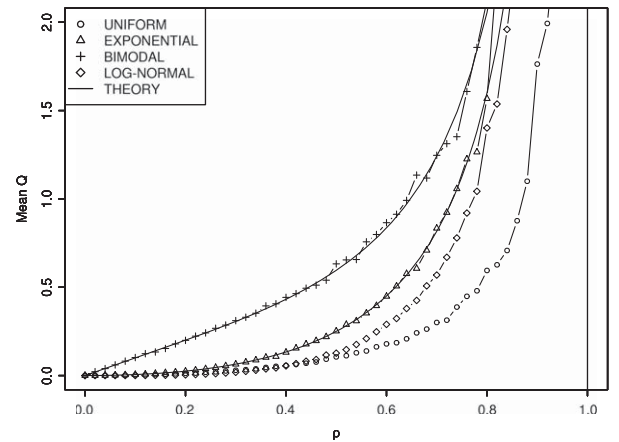


Figure 4. Mean runoff as a function of rainfall ρ . Theoretical results in black solid lines for the bimodal and exponential cases.

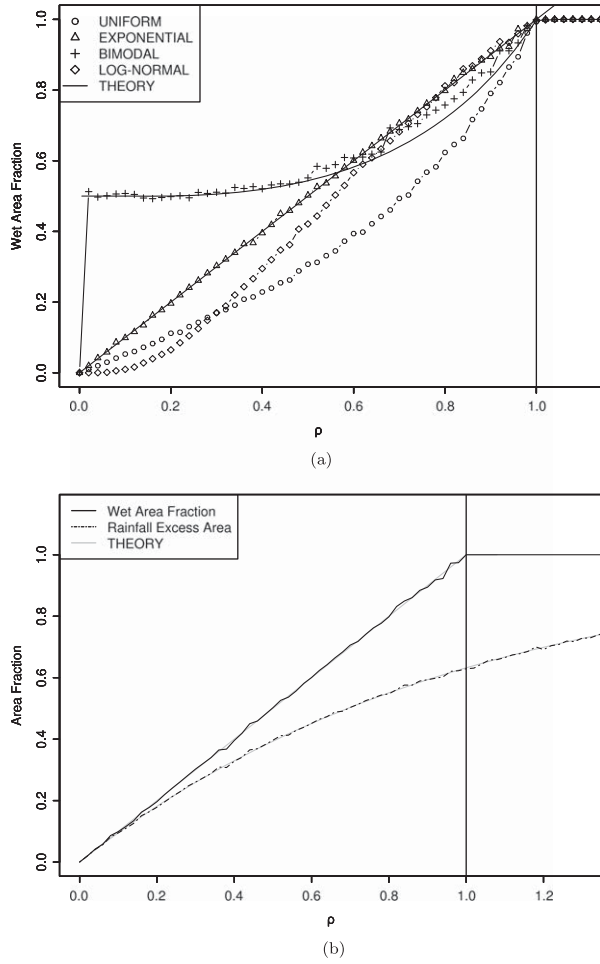


Figure 5. (a) Wet area fraction for rainfall $0 < \rho < 1$. Theoretical results displayed in black solid lines for the bimodal and exponential cases. (b) Wet area fraction compared to rainfall excess area in the exponential case. Theoretical results in grey for both quantities.

observation remains true for the other variables described below, and it explains the ordering of the four laws when ρ is small ($\rho < 0.3$).

[71] Finally, we can see that the $M/D/1$ model and the $2D/D/1$ extrapolated theory agree well with the simulations. This indicates that ergodicity is reached: the domain is long enough and no sampling issues arise, at least not when ρ is not too close to one. The few discrepancies observed for values of ρ close to one are issues of sampling and the influence of the boundary condition. They can be reduced by simulating longer slope lengths. Indeed, for ρ close to one, wet areas spread and become larger and larger, meaning that the range of influence of the boundary condition increases. Whatever the quantity considered, these issues arise whenever ρ tends to one.

[72] For $\rho > 1$ the entire slope is flooded; the mean runoff flow rate becomes linear and is no longer influenced by the infiltrability distribution.

[73] Figure 5a displays the wet area fraction ω_Q as a function of ρ . As predicted by equation (8), the fraction increases linearly for the exponential law. In the lognormal case, ω_Q evolves in the same way: it is lower than in the

exponential case for $\rho < 0.5$, with a null derivative at $\rho = 0$, and reaches unity almost linearly when $\rho \rightarrow 0$.

[74] The bimodal law exhibits the strongest-shaped and original wet area fraction. The bimodal wet area fraction starts at $\rho = 0^+$, with the probability value of the mode $I_A = 0$ ($\alpha = 0.5$ in these simulations). It is almost constant and equal to this value until $\rho \simeq 0.5$, and then increases quasi-linearly to reach unity. This behavior is easily explained. At the value $\rho = 0^+$, all of the I_A pixels produce runoff and become wet: 50% of the slope is flooded. Runon occurs in a I_B pixel ($I_B = 2$) when R is such that n consecutive I_A upstream pixels produce a runoff flow rate nR such that $(n+1)R > I_B$. Because the probability of a sequence of n consecutive I_A pixels is α^n , the rainfall rate must be high enough to produce runon which contributes to the wet area fraction. Figure 5 shows that $\rho \simeq 0.5$ seems to be a threshold value and that the corresponding number of I_A pixels is $n = 3$. Indeed, as soon as ρ exceeds 0.5, even a single non-infiltrating pixel flanked by two I_B pixels will overflow onto the next downslope pixel. The $2D/D/1$ extrapolated results provide a good approximation of the simulated wet fraction. When $\rho > 1$, $\omega_Q = 1$ for any infiltrability distribution (flooded slope).

[75] Figure 5 shows that the wet area fraction is one of the hydrological variables that best reflects the nature of the statistical law of infiltrability.

[76] To illustrate the importance of the runon process, we compare in Figure 5b the simulated wet area fraction with the rainfall excess area fraction in the exponential case, where $\omega_I(\rho) = 1 - \exp(-\rho)$. We see that when $\rho \rightarrow 1$, the runon process accounts for 40% of the wet area and, in accordance with equation (23), both fraction become identical when $\rho \rightarrow 0$.

[77] The probability density functions (pdfs) of the runoff flow rate are given in Figure 6 for $\rho = 0.4$ and $\rho = 0.8$. They are compared with the underlying infiltrability pdfs in grey. The pdfs of the flow rate are made up of three parts: a peak centered on $Q = 0$ that accounts for the “dry” pixels, and two parts defined over the ranges $0 < Q < \rho$ and $Q > \rho$. This separation is not obvious for the bimodal distribution. The integral of the last two parts is the wet area fraction. When $\rho \rightarrow 0$, the third part of the pdfs becomes negligible and the sum of the first two parts tends to the pdf of $R - I$. This inheritance of structure is especially visible in the uniform case. The pdfs of Q for the exponential, uniform and lognormal distributions seem to be discontinuous at $Q = \rho$ with high probability values for $0 < Q < \rho$ and low ones for $Q > \rho$. From a mathematical point of view this discontinuity is proved only for the exponential law [Erlang, 1909] (equation (4)). Nevertheless, one sees that the function $g(x - y)$ in the Lindley integral (equation (3)), which is the pdf of $R - I$, reads $g(x) = i(R - x)$ where $i(y)$ is the pdf of I . Therefore, R is certainly a critical value in the definition of the flow rate’s cumulative distribution function $Pr(Q < X)$ and for the pdfs of all the distributions we studied. We discuss the structure of these pdfs quantitatively in Appendix B.

[78] The pdf of the runoff flow rate for the bimodal distribution is multimodal (Figure 6d). Depending on the I_B/R value, I_B being the maximum infiltrability, there are either one or two mode populations. If R is a multiple of the maximum infiltrability, that is, $NR = I_B$ where N is an integer, then all of the modes are multiples of R . These are the

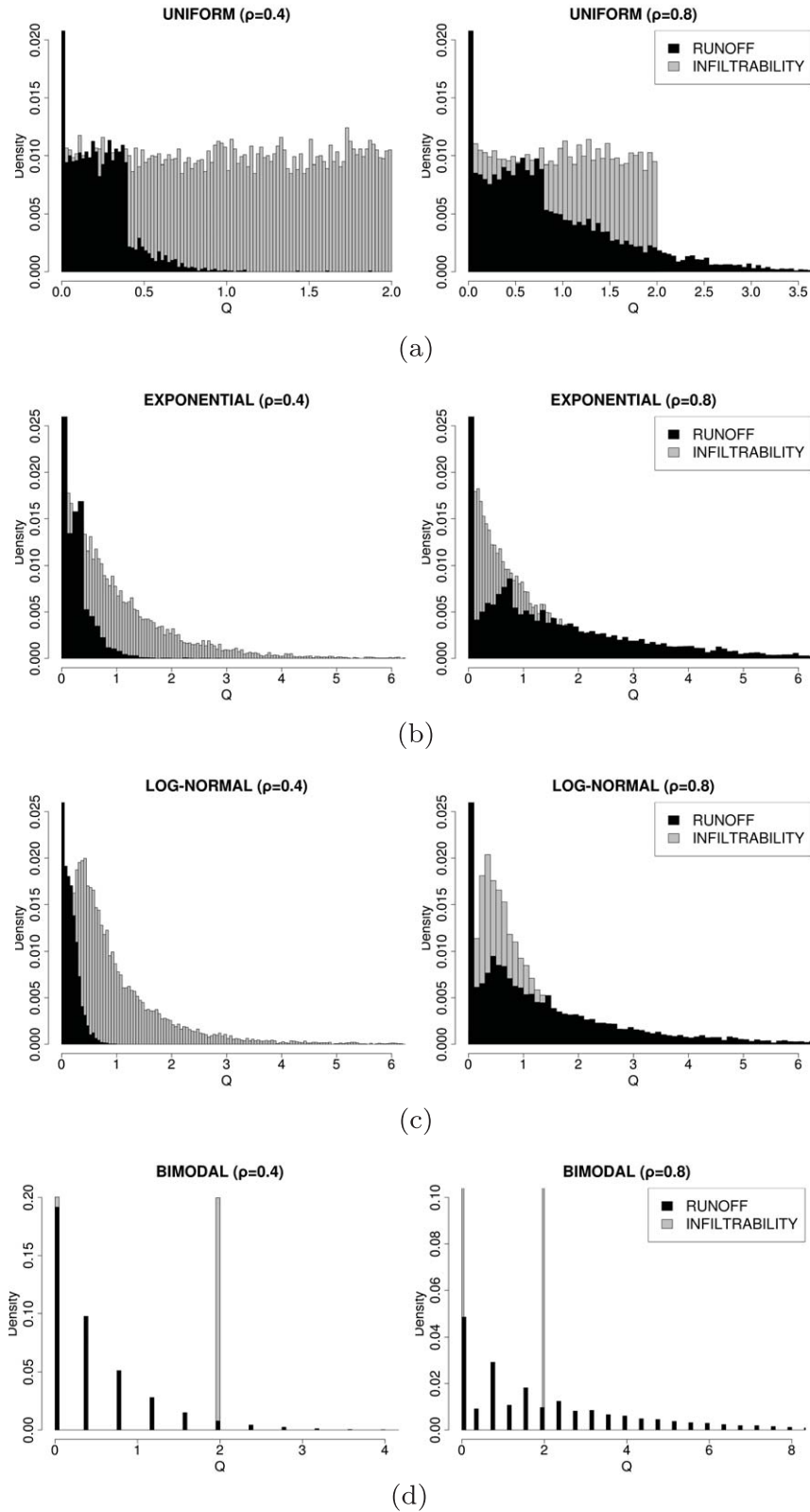


Figure 6. Probability density function (pdf) of runoff compared to the pdf of infiltrability, for rainfall (left) $\rho = 0.4$ and (right) $\rho = 0.8$. Some distribution tails and probabilities of dry pixels ($Pr(Q = 0)$) have been truncated to improve readability.

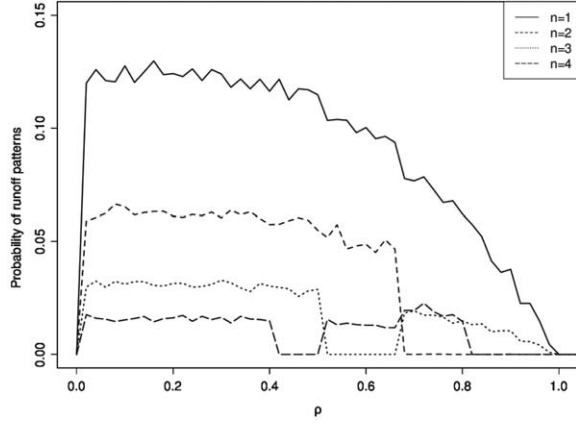


Figure 7. Probability of runoff pattern lengths ($n = 1, 2, 3$ and $4\Delta x$) for the bimodal distribution and as a function of rainfall ρ .

principal modes: $Q = nR$ with $n = 0, 1, \dots$. Otherwise, a second population appears between modes nR and $(n+1)R$ (with $n = 0, 1, \dots, N$), which is described by submodes smaller than R . These submodes depend on the fractional part of the ratio I_B/R called r , N being the integer part ($I_B = NR + r$). We conjecture that the modes and submodes are all multiples of the greatest common divisor of R and r ($\gcd(R, r)$), provided that R and I_B are integers (or decimal numbers). A partial demonstration of these results is given in Appendix B.

[79] Two examples are shown in Figure 6d to illustrate this structure in modes and submodes. For $\rho = 0.4$, we have $I_B/R = 5$ ($I_B = 2$ and $R = \rho$ in the simulations). Because I_B/R is an integer, only the principal modes are produced, and all of these are multiples of $\rho = 0.4$. When $\rho = 0.8$ (Figure 6d on the right) $I_B/R = 2.5$, that is, $N = 2$ and $r = 0.5R = 0.4$. All of the modes and submodes appearing are multiples of $\gcd(0.8, 0.4) = 0.4$. Another illustrative example is $\rho = 0.7$, in which case we find $\gcd(0.7, 0.3) = 0.1$, and the submodes as they appear along the slope are 0.3, 0.6, 0.9, 0.2, 0.5, 0.8, 0.1, 0.4, and 0.7 (see Appendix B).

3.3. Patterns and Connectivity

[80] The statistics of the wet zones lengths are described by the probabilities $P_Q(n, \rho)$ (equation (9) for the general case, and equation (10) for the exponential distribution), where $n\Delta x$ is the length of the considered wet zone. According to equation (10), the runoff patterns are less and less probable as their lengths increase, which is true for any given rainfall rate. Whatever the pattern length, all of the probabilities tend to zero when $\rho \rightarrow 1$: the wet zones coalesce into a single infinite zone.

[81] In Figure 7, the probability $P_Q(n, \rho)$ for the bimodal infiltrability distribution is displayed for n ranging from 1 to 4. The behavior of the probability is similar to that of the exponential case, though some new features appear. For $n = 2, 3, 4$ the wet patterns do not appear for some particular ranges of the rainfall rate: the associated probability is null. Such discontinuities for the bimodal case have been already noted in the study of the flow rate pdf (Figure 6). To explain this, let us consider a sequence of N pixels where the first one is dry, the N following are $I_A = 0$ and

the $N+1$ is $I_B = 2$. When $N = 1$ the sequence gives rise to a single wet pixel as long as $\rho < 2$, and $P_Q(1, \rho) = \overline{\omega}\alpha\beta$. For $N = 2$, $P_Q(2, \rho)$ becomes null when rainfall exceeds $2/3$. Indeed, the sequence generates a runoff rate of 2ρ flowing onto the third pixel. The runoff over this pixel (2ρ runoff + ρ rainfall input) infiltrates entirely unless $\rho > 2/3$. If it is, the two wet pixels pattern cannot occur but a three pixels zone may, and $P_Q(2, \rho) = \overline{\omega}\alpha^2\beta$. No other configuration could possibly generate runoff patterns of 2 pixels length, this is the reason why $P_Q(2, \rho)$ as plotted in Figure 7 is null for $\rho > 2/3$. The same reasoning also holds for different values of I_B , I_A , α , and β . Applying this analysis to higher values of N explains the absence of wet patterns for specific values of rainfall intensity.

[82] The observations made on $P_Q(n, \rho)$ in the exponential case extend to the uniform and lognormal distributions. Only the shape of the curves and their tangents at the origin differ. To compare all of the distributions, we plotted in Figure 8a the mean number of runoff patterns per unit length $\langle N_Q \rangle$ for each one of them. This quantity is simply the sum over n of $P_Q(n, \rho)$ and its expression for $M/D/1$ is given by equation (12). As in Figure 5, we observe that the

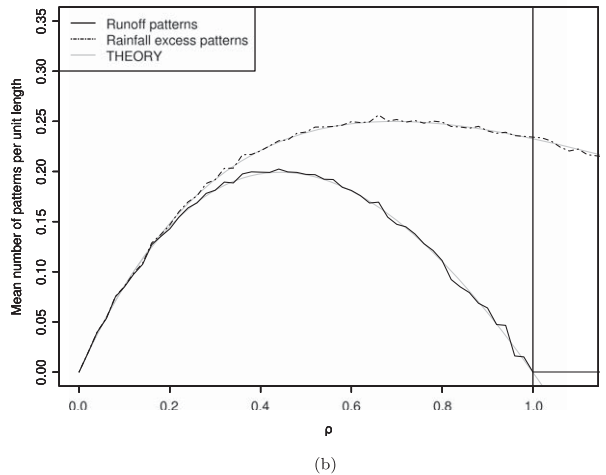
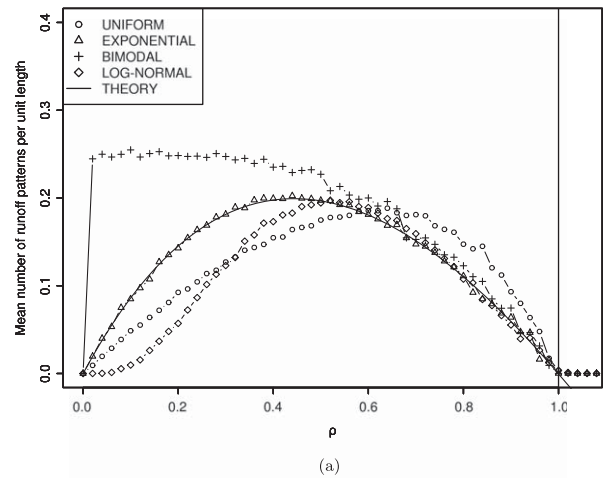


Figure 8. (a) Mean number of runoff patterns per unit length for all the distributions (theory = black solid line); (b) mean number of runoff and rainfall excess patterns for the exponential distribution (theory = gray solid lines, rainfall ρ).

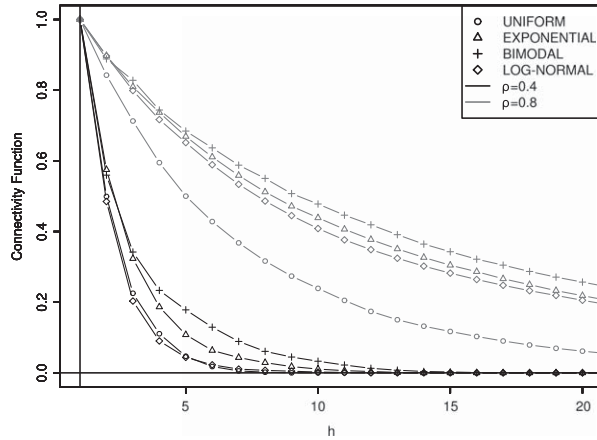


Figure 9. Connectivity function as a function of distance h , for rainfall $\rho = 0.4$ (black) and $\rho = 0.8$ (gray).

mean number of patterns for the bimodal distribution is almost constant until $\rho \simeq 1/2$. Indeed, for $\rho = 0^+$ all the $I_A = 0$ pixels are wet and $\langle N_Q \rangle = \langle N_I \rangle$, where $\langle N_I \rangle$ is mean number of rainfall excess patterns. The slope is covered by numerous small runoff patterns that begin to widen as ρ increases and connect to each other when the threshold $\rho \simeq 1/2$ is reached.

[83] For the other distributions of infiltrability, the maximum number of runoff patterns occurs for $\rho \simeq 0.6$. Runoff is organized in rather small size and isolated runoff patterns for low values of ρ . When $\rho \rightarrow 0$, $\langle N_Q \rangle \rightarrow \langle N_I \rangle \rightarrow 0$. As rainfall increases, more patterns appear and merge under the effect of runoff. The $\rho \simeq 0.6$ value (“critical rainfall”) corresponds to the preponderance of runoff and connectivity over pattern generation. Eventually, the mean number of runoff patterns decreases and tends to zero as $\rho \rightarrow 1$ (one single infinite runoff pattern).

[84] The critical rainfall is different for each distribution of soil infiltrability. Its value is high for the uniform (above $\rho = 0.6$), and low for the exponential distribution (approximately 0.4). In other words, the exponential distribution is structurally more favorable to the runoff process and the aggregation of runoff clusters than the uniform distribution.

[85] The horizontal tangent observed at $\rho = 0$ for the log-normal distribution is also present in Figures 4 and 5, for instance. This property is related to the null probability of $I = 0$ pixel occurrences: when $\rho \rightarrow 0$, no runoff is produced in the lognormal case. The shape of the curve as $\rho \rightarrow 0^+$ is determined by the scarcity of pixels with low infiltrability. Thus, the shape would be modified if the domain length was increased.

[86] We plotted $\langle N_Q \rangle$ and $\langle N_I \rangle$ for the exponential case in Figure 8b. The observed differences demonstrate the importance of the runoff process. As runoff contributes to connecting wet zones, $\langle N_Q \rangle$ decreases with ρ much more rapidly than $\langle N_I \rangle$ and the inequality $\langle N_Q \rangle < \langle N_I \rangle$ is always verified. For $\rho < 0.2$ we have $\langle N_Q \rangle \sim \langle N_I \rangle$. The theoretical expressions given by equations (12) and $\langle N_I \rangle = P^+ P^-$ in section 2.3 agree well with the simulation.

[87] Figure 9 displays the connectivity function of the runoff flow rate $\tau_Q(h)$ for each infiltrability distribution and for two specific rainfall intensities: $\rho = 0.4$ and $\rho = 0.8$. As expected, the connectivity function is maximized and equal

to unity when $h = 1$. As h increases, it drops to zero at a rate that depends on the distribution. Low rainfall rates mean small and scarce runoff patterns, and therefore, short potential connected distances. When $\tau_Q(h)$ drops to zero at a given critical h_c value, there is no wet pattern occurrence of a length greater than h_c . For small rainfall intensities ($\rho = 0.4$), the decrease of $\tau_Q(h)$ with h is exponential, as demonstrated theoretically by equation (18). When $\rho \rightarrow 1$, $h_c \rightarrow \infty$ and the connectivity function tends toward unity for any separation distance h .

[88] Also of interest in Figure 9 is the renewed observation of a hierarchy among the distributions, as first observed in Figure 4. This correspondence is expected, because high runoff pattern connectivity understandably leads to high mean runoff flow rates, and vice versa. Similar observations were found by *Western et al.* [2001], who studied the connectivity of soil moisture patterns by means of the connectivity function.

[89] The integral connectivity scale (L_{τ_Q} , equation (13)) synthesizes the connectivity characteristics over the whole range of ρ . In the present discrete version of the runoff-runon problem, the integral scale varies between zero, when no runoff is produced, and infinity (or domain length) when there is one infinite runoff pattern (connectivity function tends to unity). The smallest nonnull value of L_{τ_Q} is unity since $\tau(h > 1, \rho) \rightarrow 0$ as $\rho \rightarrow 0$, and $\tau(0, \rho) = \tau(1, \rho) = 1$ whatever the value of ρ (see the discussion after equation (16)).

[90] Comparing L_{τ_Q} and L_{τ_I} in Figure 10 proves that the pattern connectivity is greatly increased for Q , thanks to the runoff process. For $\rho = 0.5$, the integral connectivity scale for the wet area (L_{τ_Q}) already double the value of L_{τ_I} . We also compare the two theoretical approximations of L_{τ_Q} proposed in section 2.3. Approximation 1 corresponds to the assumption of independent wet pixels given by equation (17). The spatial aggregation of wet pixels into patterns that allows runoff accumulation (and pattern connectivity) is neglected. As a consequence, approximation 1 greatly underestimates the simulated functional connectivity scale.

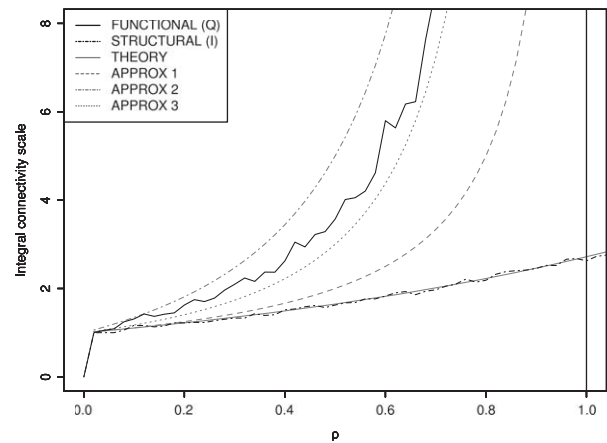


Figure 10. Functional and structural integral connectivity scale, for the exponential distribution. Exact theoretical results in gray solid lines. Approximation 1 is given by equation (17), approximation 2 by equation (20), and approximation 3 corresponds to equation (24) (Rainfall ρ).

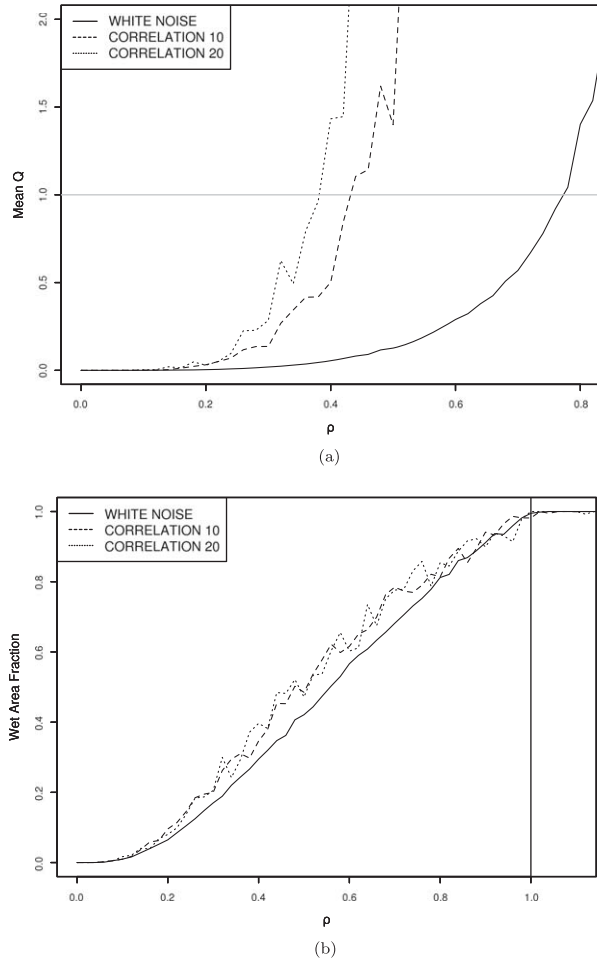


Figure 11. Lognormal correlated distribution: mean runoff (a) and wet area fraction (b) for two correlations ($\lambda = 10\Delta x$ and $20\Delta x$) and the uncorrelated case (white noise) (Rainfall ρ).

[91] Surprisingly, approximation 2 (equation (20)) produce a curve above the simulated one. According to section 2.3, this is contrary to what we expected. To clarify this point, we consider the connectivity function as defined by Stauffer (equation (22)) and derive the following expression of $L_{\tau_Q}^*$ for the 1-D geometry:

$$L_{\tau_Q}^* = \frac{1}{2} \left(1 + \frac{\langle l_Q^2 \rangle}{\langle l_Q \rangle} \right) \quad (24)$$

where l_Q is the length of a wet pattern. This expression, denoted approximation 3 in Figure 10, gives the expected curve, which is close to the simulated one. We believe that the integral connectivity scale expression of Renard and Allard [2011] (approximation 2, equation (20)) applies instead to 2-D and 3-D geometries.

3.4. Correlated Infiltrability and Nugget Effect

[92] The numerical results obtained with a correlated lognormal infiltration are summarized in Figure 11. Figures 11a and 11b show the mean runoff flow rate and the wet area fraction, respectively, for both the uncorrelated

and correlated cases. The covariance is exponential and two correlation lengths have been considered $\lambda = 10\Delta x$ and $\lambda = 20\Delta x$. The latter value has been frequently adopted, for instance, by Corradini *et al.* [1998] in Monte-Carlo simulations of runoff-runon on soils with a lognormal hydraulic conductivity. An increase in the infiltration correlation leads to a much higher mean runoff production. The impact of correlation on the mean flow rate is explained as follows: on a low infiltration zone, the runoff flow rate grows linearly on a distance of the order of the correlation length and then decreases in the next high infiltration zone. As a consequence, the mean flow rate increases with the scale of the correlation. Our results suggest that increasing the autocorrelation in the infiltration field results in higher functional (and structural) connectivity and thus more production of runoff on average. This is in agreement with the conclusions presented by Michaelides and Wilson [2007].

[93] On the other hand, the wet area fraction is not very dependent on the correlation: when the lengths of the rainfall deficit areas ($R < I$) increase because of correlation, the lengths of the rainfall excess areas ($R > I$) also increase for the same reason. If one considers a periodic infiltration variability, for instance, one may easily show that the wet area fraction does not depend on the period.

[94] Our simulations agree with Tin [1985] results, though the correlation definition is not equivalent (refer to section 2.2). The mean and the variance of the runoff flow rate may be computed from the runoff distribution derived by Tin, which depends on the correlation coefficient κ (see equation (7)). The results show that the mean flow rate increases with κ for a given rainfall rate. For $\rho = 0.5$, $\langle Q \rangle_{(\kappa=0.9)} \simeq 2\langle Q \rangle_{(\kappa=0)}$ and for $\rho = 0.8$, $\langle Q \rangle_{(\kappa=0.9)} \simeq 10\langle Q \rangle_{(\kappa=0)}$. Tin also suggested that there was little influence of correlation on the wet area fraction.

[95] To further develop this work, we studied the impact of a nugget effect. A nugget accounts for uncorrelated measurement errors and/or variations at scales much smaller than the pixel scale. The addition of a white noise to the log of infiltration leads to sampling problems. The domain must be quite large ($> 10^7$ pixels) to obtain the expected statistical means with a good precision simply by spatial averaging. As this constraint requires considerable computing resources, we decided to simplify the problem and studied the influence of a nugget added to a sinusoid (i.e., deterministic) infiltration distribution:

$$I(p, x) = I_0 + \sqrt{(1-p)} \cos(2\pi x/\theta) + \sqrt{p} \psi \quad (25)$$

where p is the nugget ($0 \leq p \leq 1$), $I_0 = 1$ is the mean infiltration, θ is the period ($\theta = 20$ pixels in the simulation) and ψ is a Gaussian white noise of null mean and a variance of unity. When $p = 0$ the infiltration is a simple sinusoid, and as p increases the infiltration signal shifts toward a pure Gaussian white noise (eventual negative values are set to zero). The underlying assumptions in our choice of sinusoidal infiltration are: (i) the influence of a nugget does not depend heavily on the nature of the initial infiltration signal; and (ii) the Fourier transform of a random signal is a superposition of sinusoids. The runoff flow rate progressively loses its periodic structure as p increases.

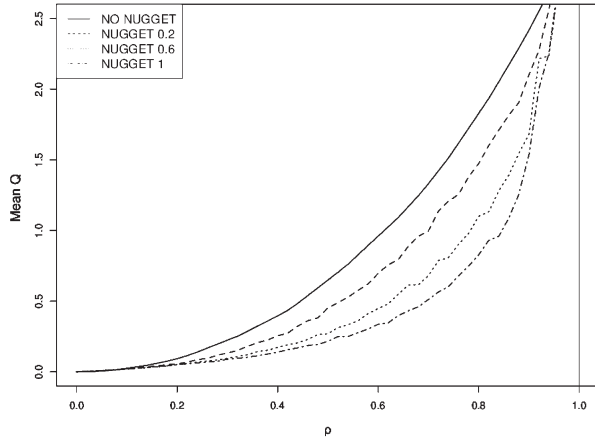


Figure 12. Mean runoff for different values of nugget as a function of rainfall ρ , for a sinusoidal distribution of infiltrability.

However, the mean and variance of runoff undergo a limited diminution for most ρ (Figure 12). If the statistical moments of runoff vary feebly with the nugget effect, this is obviously not the case of the runoff pattern statistics. Our preliminary results show that subscale heterogeneity may have an impact on runoff generation, especially on the length and number of the runoff patterns. *Michaelides and Wilson* [2007] found similar results, namely that the addition of a nugget to soil infiltrability diminishes the functional connectivity because fewer runoff patterns are generated (and less runoff is produced).

3.5. Influence of Boundary Condition and Scale Effect

[96] The inflow boundary condition in pixel $i=1$, $Q_0=0$, influences the spatial distribution of the runoff flow rate up to a certain distance L_{stat} beyond which Q becomes stationary. To study the convergence of the mean flow rate $\langle Q \rangle$ to its stationary state for the four uncorrelated infiltrability distributions, we considered only the first 100 pixels of the domain and performed 2.10^5 Monte-Carlo simulations. We define L_{stat} as the distance at which the mean flow rate is equal to 95% of its asymptotic value (equation (5), for $M/G/1$).

[97] The lengths L_{stat} (not presented here) follow the same hierarchy as the connectivity function (Figure 9): uniform < lognormal < exponential < bimodal. This is not surprising because the more the wet areas are connected, the longer the distance to reach a stationary state. For $\rho \simeq 0.5$, the distance associated to the bimodal is four times greater than that of the uniform distribution. All the distances increase indefinitely when $\rho \rightarrow 1$, which indicates that a stationary state cannot be established.

[98] In queuing theory, authors usually prefer to work in the continuous-time framework and define T_{stat} as the relaxation time, i.e., the time it takes to reach a given percentage of the mean stationary waiting time [see *Novak and Watson*, 2009, for $M/D/1$]. Unfortunately the transformation of T_{stat} into L_{stat} is not straightforward. *Kelton and Law* [1985] proposed numerically solved expressions in the discrete-time framework for $M/M/1$. This theoretical approach should apply to any queue with independent distributions of interarrival and service times.

[99] Some authors attribute the observed scale dependency of the runoff coefficient, i.e., the decrease in the runoff coefficient with domain size, to both spatial variability of infiltration rate and the runoff process. Let us consider a subdomain of extent ℓ in our 1-D domain, located far from the zero-flow boundary condition imposed at the top ($x \gg L_{stat}$). It is clear that when $\rho < 1$, the runoff stationary state on the subdomain leads to a mean runoff coefficient of $C_Q = \langle Q \rangle / R\ell$, decreasing with ℓ . When $\rho > 1$, the mean runoff coefficient is constant and independent of ℓ , $C_Q = 1 - 1/\rho$. Remember that when $\rho > 1$, the mean runoff flow rate grows linearly with the slope length l , $\langle Q_l \rangle \sim (R - \langle I \rangle)l$ where $l \gg 1$. For $\rho < 1$, the coefficient decreases rapidly, as the inverse of the domain size. Such a decrease has not been observed by the authors who support the scale effect theory [*Cerdan et al.*, 2004; *Gomi et al.*, 2008]. We suggest that the slow decrease observed on-site and the apparent independence from the rainfall rate may come from the influence of the zero flow upper boundary condition on the mean runoff flow rate, near the top of the domain. This influence was the reason we discarded the 2000 upslope pixels in all our previous simulations.

[100] To prove this assertion, we define the runoff coefficient $C_Q(\rho, l)$ as the ratio between $\langle Q_l \rangle$, the mean runoff flow rate at $i=l$, and lR the rainfall volume received per unit time on the l first pixels. Figure 13 displays the evolution of the runoff coefficient as a function of l for $\rho = 0.4, 0.8, 1.2$, and 1.6 for the exponential case. We observe that as the distance from the upslope boundary (l) increases, C_Q decays more slowly than $1/l$ when $\rho < 1$. According to the previous observations on L_{stat} , the convergence of C_Q to its stationary value, zero for $\rho < 1$, occurs over short distances when $\rho \ll 1$.

[101] When $\rho > 1$, runoff increases linearly with the slope length, so the runoff coefficients tend to the stationary value $1 - 1/\rho$. A decrease of $C_Q(\rho, l)$ with l is still observed as long as ρ is close to one. When ρ increases, the runoff coefficient rapidly reaches its stationary value (see $\rho = 1.6$ in Figure 13), and our model no longer accounts for the scale effect.

[102] It is worth mentioning that a scale effect was observed in Figure 4a even without the boundary condition influence and for $\rho < 1$. Lognormal distributions

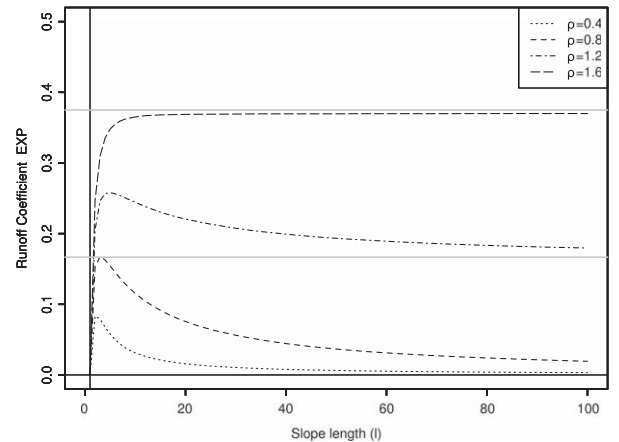


Figure 13. Runoff coefficient in the exponential case for different values of ρ and as a function of slope length l .

(characteristic of hillslope scales) generate less runoff than exponential ones (plot scale).

[103] The analysis of the runoff coefficient provides an answer to the question posed by *Hawkins and Cundy* [1987] about the mean infiltration rate of a system composed of homogeneous parallel strips orthogonal to the slope. As discussed in section 1, these authors showed that for a system of parallel strips aligned along the slope and with exponentially distributed strip infiltrabilities, the mean infiltrability $\langle i \rangle$ increases with the rainfall rate as $\langle i \rangle(\rho) = 1 - \exp(-\rho)$. We found that for strips orthogonal to the slope, the mean infiltrability is a piecewise function of ρ : $\langle i \rangle(\rho) = \rho$ for $\rho < 1$ and $\langle i \rangle(\rho) = 1$ for $\rho > 1$. This result is independent of the infiltrability distribution.

4. Conclusion

[104] We studied the statistical characteristics of the steady state runoff produced during a constant and uniform rainfall event, R , on a 1-D flat slope with random infiltrability, I , using queuing theory and the connectivity framework. Four uncorrelated infiltrability distributions (exponential, bimodal, lognormal, uniform) and one correlated (lognormal) were considered.

[105] We showed that, whatever the distribution, when rainfall is low compared to the mean infiltrability, runoff is produced in the rainfall excess zones (i.e., zones where $R > I$). When R increases, runoff takes place: the wet zones become larger than the rainfall excess zones, wet patterns connect and runoff connectivity increases. As the rainfall rate tends toward the mean infiltrability $\langle I \rangle$, the patterns coalesce into a single infinite pattern and the entire slope becomes flooded. Consequently, most of the statistical quantities describing runoff, such as the mean flow rate, are nonlinear functions of R . We found that the importance of runoff patterns and their connectivity decreases as $R \rightarrow \langle I \rangle$. When R exceeds $\langle I \rangle$, the structure of the infiltrability distribution becomes unimportant.

[106] A hierarchy among distributions in terms of flow rate and connectivity, namely bimodal > exponential > lognormal > uniform, is observed. Therefore, high runoff flow rates are produced by systems featuring high structural and functional connectivities.

[107] We derived some theoretical results, partly from solutions proposed in queuing theory, on the statistics of wet patterns and on connectivity in the exponential and bimodal cases. A general formal expression for the connectivity function, which only has an analytical expression for the structural connectivity, is also proposed. The agreement with the simulated connectivity is good. We proposed and discussed different approximations for the functional connectivity integral scale. Some of these approximations were derived by authors who did not precisely define the associated connectivity functions. As several definitions are currently used in the literature, we could not decide which approximation was the most appropriate for our connectivity definition. This issue should be clarified.

[108] Introducing a correlation to the infiltrability spatial structure significantly increases the flow rate but not the wet area fraction. On the contrary, a nugget reduces the mean flow rate and connectivity accordingly. A zero flow upslope boundary condition influences the runoff flow

rate's statistical moments over distances close to this boundary. We propose that the scale effect on the runoff coefficient, i.e., the decrease in runoff coefficients with the scale of observation, can be explained as a consequence of this boundary influence on the mean flow rate. The mean infiltrability is found to be a piecewise function of R and independent of the infiltrability distribution.

[109] The runoff model used in this work relies on the following assumptions: 1-D slope, constant, and uniform rainfall, runoff at steady state, infiltration rate constant over time, no influence of the subsurface. This last assumption is essential for the application of the queuing theory. For this reason and according to the discussion of section 1, the plot-scale simulated rainfall experiment represents the nominal situation to which the model applies. At a larger scale the assumption may be also justified in regions where Hortonian overland flow dominates and the water table is deep. This is the case of semiarid areas (shrublands) [e.g., *Howes and Abrahams*, 2003] or agricultural lands in temperate climate. Semiarid areas are characterized by sandy soils with sparse vegetation and runoff is generally produced by excess infiltration. The base flow is often absent and the water table is typically below stream beds and disconnected from surface runoff [*Pilgrim et al.*, 1988]. Agricultural lands in temperate climate, the plateaus of the northwestern European loess belt [*Evrard et al.*, 2010], may also verify the assumption of surface-subsurface decoupling. The water table is usually several meters deep and because of surface crusting and sealing Hortonian runoff dominates [*Cerdan et al.*, 2002].

[110] According to *Dunne* [1978], runoff is seldom produced in humid regions with important vegetation cover, principally because infiltration capacities are so high that few rainstorms have sufficient intensities to exceed them. When the aquifer is shallow the subsurface and surface are often connected. For these different reasons, our model should not apply to this type of environment.

[111] While remaining in the queuing theory framework, we may reasonably think that the other assumptions, 1-D slope, constant rainfall, and runoff at steady state, will be relaxed in the future. The 1-D transient rainfall case is quite complex and no theoretical framework has been proposed until now. Preliminary studies show that the queuing theory is still applicable but requires some assumptions about the nonlinearity of the runoff transport equation.

[112] When the flow is unidimensional, i.e., runoff may only flow to the immediate downslope pixel, the extension of the present work to a 2-D flat geometry is straightforward, at least for uncorrelated infiltrability distributions (parallel, independent heterogeneous strips model). If transverse transport is introduced, i.e., runoff may flow in the immediate downslope pixel but also in the two neighboring downslope pixels, the runoff-runon physics becomes fully 2-D (and difficult to predict). One might expect the introduction of a second dimension to increase the connectivity of both infiltrability and runoff fields. An important question that 2-D simulations should be able to answer is whether the mean infiltration rate may or may not be framed by the parallel homogeneous strips and the parallel heterogeneous strips models (strips aligned along the slope). We will address these issues in a forthcoming paper (submitted) and show that percolation theory is a valuable framework to analyze and quantify the 2-D connectivity.

Appendix A: Bimodal Infiltrability, Uniform Rainfall Rate (2D/D/1)

[113] We consider a domain with a bimodal infiltration distribution: I_i may be equal to I_A with probability α , or I_B with probability β ($\alpha + \beta = 1$). Rainfall rate is uniform and equal to R . To simplify the notations, we introduce the variables $\delta I = I_B - I_A$, $r = (R - I_A)/\delta I$, $I_i = I_A + \delta I \eta_i$ and $q_i = Q_i/\delta I$, where η is generated by a bimodal distribution ($\eta_i = 0$ with probability α or 1 with probability β). Equation (1) is rewritten

$$q_i = (q_{i-1} + r - \eta_i)^+ \quad (A1)$$

[114] The problem is equivalent to a domain with infiltration abilities equal to either one or zero, and a rainfall rate r lying between zero and β , where the stability criteria is $\rho = R/\langle I \rangle = r/\beta < 1$.

[115] Pixels with zero infiltration may be removed from the domain as follows. Let us consider a sequence of n consecutive pixels with zero infiltration. If q_i is the runoff flow rate into the first pixel of the sequence, pixel $i + 1$, then the flow rate out of pixel $i + n$ is $q_{i+n} = q_i + nr$. Consequently, pixel $i + n + 1$ is connected with pixel i and $(n + 1)r$ may be considered as an effective rainfall rate in pixel $i + n + 1$: $q_{i+n+1} = q_i + (n + 1)r - 1$. The n pixels with zero infiltration are “transparent” in the runoff-runon dynamics. The initial problem has been transformed into a problem with a deterministic infiltration field, homogeneous and equal to one, with a random rainfall rate r' following a geometrical distribution: $P(r' = nr) = \beta \alpha^{n-1}$. This is proved as follows: the probability of a sequence of n pixels with zero infiltration framed by two pixels with a nonzero infiltration is $(1 - \alpha)^2 (\alpha)^n$. As the total number of pixels has been reduced in the transformation of the problem, passing from $N_0 + N_1$ to N_1 where N_0 and N_1 are the number of pixels with $\eta = 0$ and $\eta = 1$, respectively, the last probability must be divided by β to obtain the geometrical distribution. This new problem corresponds to the queue $D/Geo/1$ which has been studied by Roberts and Guillemin [1992]. $D/Geo/1$ is a discrete time queue where the interarrival time is constant and equal to d (we choose $d = 1$), and the service time $k = 1, 2, \dots$ is distributed geometrically with parameter p on the set of positive integers with a probability $Pr(S = k) = p(1 - p)^{k-1}$. The probability of the waiting time is:

$$Pr(W = 0) = (1 - \sigma) \quad (A2)$$

$$Pr(W = k) = \sigma(1 - \sigma)(1 - p)[1 - (1 - p)(1 - \sigma)]^{k-1}, \quad k \geq 1$$

where σ is the solution of the equation $z = (p + (1 - p)z)^d$. If $\rho < 1$, this solution exists and lies between 0 and 1. In our case (2D/D/1), because $d = 1$ and $r < 1$, the equivalence between 2D/D/1 and $D/Geo/1$ exists only for $r = 1/N$, where N is a positive integer. The probability of the runoff flow rate q' is:

$$Pr(q' = 0) = 1 - \sigma \quad (A3)$$

$$Pr(q' = k/N) = \sigma(1 - \sigma)\beta[1 - \beta(1 - \sigma)]^{k-1}, \quad k \geq 1$$

where σ is solution of $z = (\alpha + \beta z)^N$.

[116] To obtain the statistics of the initial system, we must invoke the central limit theorem. The runoff flow rate produced by the pixel located before a sequence of n pixels with

zero infiltration is distributed with the general probability given by equation (A2). After a development that we do not present here (paper submitted), this theorem leads to the probability of the runoff flow rate in the initial system. We give only the expressions of the two first moments of the flow rate q :

$$\langle q \rangle = \langle q' \rangle + \sum_{n=1}^{\infty} \alpha^n \beta^2 \left(n \langle q' \rangle + \frac{n(n+1)}{2} r \right) \quad (A4)$$

$$= \langle q' \rangle + \frac{\alpha}{1 - \alpha} r$$

and

$$\langle q^2 \rangle = \langle q'^2 \rangle (\beta + A) + B \langle q' \rangle r + C r^2 \quad (A5)$$

$$A = \beta + \alpha \beta + 2\alpha^2$$

$$B = 2\alpha \beta + \alpha^2 + 6\alpha^2 \beta + 4\alpha^3$$

$$C = 4\alpha \beta + 2\alpha^2 + 21\alpha^2 \beta + 8\alpha^3 + 16\alpha^3 \beta + 8\alpha^4$$

where $\langle q' \rangle$ is the mean runoff flow rate in the reduced system. $\langle q' \rangle$ and $\langle q'^2 \rangle$ are given by the relationships:

$$\langle q' \rangle = \frac{r}{\beta} \left(\frac{\sigma}{1 - \sigma} \right) \quad (A6)$$

$$\langle q'^2 \rangle = r^2 \sigma \left(\frac{2}{\beta(1 - \sigma)} - 1 \right)$$

[117] The first term in the expression of the mean flow rate (equation (A3)) represents the mean flow rate in the transformed system, and the second one (sum) represents the mean flow rate in the domain with zero infiltration pixels. The term $\alpha^n \beta^2 (n \langle q' \rangle + n(n+1)r/2)$ is the contribution of the sequence of n zero infiltration pixels framed by two pixels with nonzero infiltration.

[118] It is easy to see that the wet area fraction is:

$$Pr(q \neq 0) = \alpha + \beta \sigma \quad (A7)$$

Appendix B: Probability Density Function of Q

6.1. Exponential, Uniform, and Lognormal Distributions

[119] To explain the structure of the runoff flow rate pdfs for the exponential, uniform, and lognormal distributions, let us consider the sequences, i.e., realizations, of pixels such that the first pixel is dry, $Q_0 = 0$, and the followings are wet, $Q_{n \geq 1} > 0$. It is clear that Q_n cannot exceed nR , and $Q_n = nR$ if $Q_{n-1} = (n-1)R$ and $I_n = 0$, condition equivalent to $I_1 = I_2 = \dots = I_n = 0$. The pdf of Q_n , $p_n(Q)$, is given by Lindley integral (equation (3)) rewritten for each pixel (no stationary assumption):

$$p_n(Q) = \int_0^{(n-1)R} p_{n-1}(Q') i(Q' - Q + R) dQ' \quad (0 < Q \leq R) \quad (B1)$$

$$p_n(Q) = \int_{Q-R}^{(n-1)R} p_{n-1}(Q') i(Q' - Q + R) dQ' \quad (R < Q \leq nR) \quad (B2)$$

where $p_1(Q) = i(R - Q_1) (0 < Q_1 \leq R)$ and $i(I)$ is the pdf of I . These two integrals show that $p_n(Q)$ is defined on each

interval $(k-1)R < Q \leq kR$ ($k=1, \dots, n$). With these definitions the pdf of Q is:

$$p(Q) = \sum_{k=n}^{\infty} p_k(Q) \quad (nR < Q \leq (n+1)R) \quad (\text{B3})$$

[120] When expressed in terms of $i(I), p_n(Q)$ is described by integrals of the product $i(I_1)i(I_2) \dots i(I_n)$ on the hypersurface defined by $I_1 + I_2 + \dots + I_n = nR - Q$ and $I_1 < R, I_2 < 2R, \dots, I_n < nR$. For $(n-1)R < Q \leq nR$, $p_n(Q)$ is the integral of $i(I_1)i(I_2) \dots i(I_n)$ on the hypersurface described by $I_1 + I_2 + \dots + I_n = nR - Q$ and $I_i < nR - Q$ ($i=1, \dots, n$). Therefore, one may approximate $p_n(Q = nR - \epsilon) \simeq (nR - Q)^{n-1} (i(0))^n$ where $\epsilon \ll R$. Indeed, this approximation is valid for infiltrability distributions which are nonzero for $I = 0$. When $i(0) = 0$ but $i'(0) \neq 0$ (derivative of $i(I)$ at $I = 0$), the approximation may be replaced by $p_n(Q = nR - \epsilon) \simeq (nR - Q)^{2n-1} (i'(0))^n$. The case of the lognormal distribution is particular because all its derivatives are null at $I = 0$. According to these developments, we see that $p_n(Q)$ is described by a ρ^{n-1} order expression, which shows that the pdf $p(Q)$ is discontinuous at each $Q = nR$ and decreases like ρ^n when n increases. According to equation (B3), $p(Q)$ is expressed as an expansion series in powers of ρ^k , k starting at n for $nR < Q \leq (n+1)R$. Considering the uniform distribution, the preceding expressions give $p_1(0 < Q \leq R) = 1/\langle I \rangle$ (ρ^0 term), $p_2(0 < Q \leq R) = R/\langle I \rangle^2$ and $p_2(R < Q \leq 2R) = (2R - Q)/\langle I \rangle^2$ (ρ^1 terms) and $p_n(Q = nR - \epsilon) \simeq (nR - Q)^{n-1}/\langle I \rangle^n$ (ρ^{n-1} term).

6.2. Bimodal Distribution

[121] The runoff flow rate pdf for the bimodal distribution is multimodal. To demonstrate this assertion, we consider a sequence of pixels where the first pixel is dry, the A following ones are $I_A = 0$ and the $A + 1$ is I_B . This sequence represents a wet area with a runoff production equal to $Q = R, 2R, \dots, AR$ on the noninfiltrating pixels. The associated probabilities are proportional to $\alpha, \alpha^2, \dots, \alpha^A$, respectively. On the $A + 1$ pixel, runoff is equal to $Q_{A+1} = (A+1)R - I_B$ with probability $(1-\alpha)\alpha^A$. If $A+1 \leq I_B/R$, the $A + 1$ pixel infiltrates all of the water produced by the A upslope pixels, $Q_{A+1} = 0$, and a new runoff process starts at the pixel $A + 2$. In this case, only principal modes (i.e., Q multiples of R) are generated. If $A+1 \geq I_B/R$, two cases must be distinguished depending on the ratio $I_B/R = N + r$, where N and r are the integer and the fractional parts of the ratio, respectively. If $r = 0$, the outflow of pixel $A + 1$ is always a multiple of R and only principal modes are generated. Otherwise, if I_B/R is noninteger ($r \neq 0$), the $A + 1$ pixel contributes to a new mode $Q_{A+1} = (A+1-N)R - r$. Depending on the next sequence of downslope pixels, those being either infiltrating or noninfiltrating, several submodes multiples of r or $R - r$ appear. Therefore, in this case both principal modes and submodes are generated. We conjecture that all these modes are multiples of the greatest common divisor of R and r , $\gcd(R, r)$ (or $\gcd(R, R-r)$ equivalently).

[122] **Acknowledgment.** This work has been supported by the EC2CO program of the French National Center for Scientific Research (CNRS/INSU).

References

- Adams, R., A. Western, and A. Seed (2012), An analysis of the impact of spatial variability in rainfall on runoff and sediment predictions from a distributed model, *Hydrol. Processes*, 26, 3263–3280.
- Adan, I., and V. Kulkarni (2003), Single-server queue with Markov-dependent inter-arrival and service times, *Queueing Syst.*, 45, 113–134.
- Allard, D., et al. (1993), On the connectivity of two random set models: The truncated Gaussian and the Boolean, in *Geostatistics Tróia*, vol. 92, edited by A. Soares, pp. 467–478, Kluwer Acad., Dordrecht, Netherlands.
- Antoine, M., M. Javaux, and C. Bièdiers (2009), What indicators can capture runoff-relevant connectivity properties of the micro-topography at the plot scale?, *Adv. Water Resour.*, 32, 1297–1310.
- Asmussen, S. (2003), *Applied Probability and Queues*, vol. 51, Springer, New York.
- Bhat, V. N. (1993), Approximation for the variance of the waiting time in a gi/g/1 queue, *Microelectron. Reliab.*, 33, 1997–2002.
- Bracken, L., and J. Croke (2007), The concept of hydrological connectivity and its contribution to understanding runoff-dominated geomorphic systems, *Hydrol. Processes*, 21, 1749–1763.
- Bromley, J., J. Brouwer, A. Barker, S. Gaze, and C. Valentine (1997), The role of surface water redistribution in an area of patterned vegetation in a semi-arid environment, south-west Niger, *J. Hydrol.*, 198, 1–29.
- Cammeraat, E. (2004), Scale dependent thresholds in hydrological and erosion response of a semi-arid catchment in southeast Spain, *Agric. Ecosyst. Environ.*, 104, 317–332.
- Casenave, A., and C. Valentin (1992), A runoff capability classification system based on surface features criteria in semi-arid areas of West Africa, *J. Hydrol.*, 130, 231–249.
- Cerdan, O., V. Souchère, V. Lecomte, A. Couturier, and Y. Le Bissonnais (2002), Incorporating soil surface crusting processes in an expert-based runoff model: Sealing and transfer by runoff and erosion related to agricultural management, *Catena*, 46, 189–205.
- Cerdan, O., Y. Le Bissonnais, G. Govers, V. Lecomte, K. Van Oost, A. Couturier, C. King, and N. Dubreuil (2004), Scale effect on runoff from experimental plots to catchments in agricultural areas in Normandy, *J. Hydrol.*, 299, 4–14.
- Corradini, C., R. Morbidelli, and F. Melone (1998), On the interaction between infiltration and Hortonian runoff, *J. Hydrol.*, 204, 52–67.
- Daley, D. (1968), The serial correlation coefficients of waiting times in a stationary single server queue, *J. Aust. Math. Soc.*, 8, 27.
- Darboux, F., P. Davy, and C. Gascuel-Oudoux (2002a), Effect of depression storage capacity on overland-flow generation for rough horizontal surfaces: Water transfer distance and scaling, *Earth Surf. Processes Landforms*, 27, 177–191.
- Darboux, F., C. Gascuel-Oudoux, and P. Davy (2002b), Effects of surface water storage by soil roughness on overland-flow generation, *Earth Surf. Processes Landforms*, 27, 223–233.
- Dunne, T. (1978), Field studies of hillslope flow processes, *Hillslope Hydrol.*, 227, 293.
- Dunne, T., W. Zhang, and B. Aubry (1991), Effects of rainfall, vegetation, and microtopography on infiltration and runoff, *Water Resour. Res.*, 27, 2271–2285.
- Erlang, A. (1909), The theory of probabilities and telephone conversations, *Nyt Tidsskr. Matematik B*, 20, 33–39.
- Esteves, M., and J. M. Lapetite (2003), A multi-scale approach of runoff generation in a Sahelian gully catchment: A case study in Niger, *Catena*, 50, 255–271.
- Evrard, O., G. Nord, O. Cerdan, V. Souchère, Y. Le Bissonnais, and P. Bonté (2010), Modelling the impact of land use change and rainfall seasonality on sediment export from an agricultural catchment of the north-western European loess belt, *Agric. Ecosyst. Environ.*, 138, 83–94.
- Feller, W. (2008), *An Introduction to Probability Theory and its Applications*, vol. 2, John Wiley, New York.
- Gomi, T., R. Sidle, S. Miyata, K. Kosugi, and Y. Onda (2008), Dynamic runoff connectivity of overland flow on steep forested hillslopes: Scale effects and runoff transfer, *Water Resour. Res.*, 44, W08411, doi: 10.1029/2007WR005894.
- Govindaraju, R., C. Corradini, and R. Morbidelli (2006), A semi-analytical model of expected areal-average infiltration under spatial heterogeneity of rainfall and soil saturated hydraulic conductivity, *J. Hydrol.*, 316, 184–194.
- Grayson, R., G. Blöschl, A. Western, and T. McMahon (2002), Advances in the use of observed spatial patterns of catchment hydrological response, *Adv. Water Resour.*, 25, 1313–1334.

- Hawkins, R., and T. Cundy (1987), Steady-state analysis of infiltration and overland flow for spatially-varied hillslopes, *Water Resour. Bull.*, 23, 251–256.
- Hillel, D. (1998), *Environmental Soil Physics: Fundamentals, Applications, and Environmental Considerations*, Academic, New York.
- Hopp, L., and J. McDonnell (2009), Connectivity at the hillslope scale: Identifying interactions between storm size, bedrock permeability, slope angle and soil depth, *J. Hydrol.*, 376, 378–391.
- Horton, R. (1935), *Surface Runoff Phenomena*, vol. 1, Edwards Brothers, Inc., Ann Arbor, Mich.
- Howes, D., and A. Abrahams (2003), Modeling runoff and runoff in a desert shrubland ecosystem, Jornada basin, New Mexico, *Geomorphology*, 53, 45–73.
- Hunter, J. (2007), Markovian queues with correlated arrival processes, *Asia-Pac. J. Oper. Res.*, 24, 593–611.
- Iliadis, I., and S. Fuhrmann (1992), Moment relationships for queues with Poisson input, *Queueing Syst.*, 12, 243–256.
- Jones, O., G. Sheridan, and P. Lane (2009), A stochastic runoff model incorporating spatial variability, in *18th World IMACS Congress and MODSIM09 International Congress on Modelling and Simulation*, edited by R. Anderssen, R. Braddock, and L. Newham, Modell. and Simul. Soc. Aust. and N. Z., Cairns, Australia.
- Kelton, W., and A. Law (1985), The transient behavior of the m/m/s queue, with implications for steady-state simulation, *Oper. Res.*, 33, 378–396.
- Kendall, D. (1951), Some problems in the theory of queues, *J. R. Stat. Soc., Ser. B*, 13, 151–185.
- Knudby, C., and J. Carrera (2005), On the relationship between indicators of geostatistical, flow and transport connectivity, *Adv. Water Resour.*, 28, 405–421.
- Konheim, A. (1975), An elementary solution of the queueing system g/g/1, *SIAM J. Comput.*, 4, 540.
- Kramer, W., and M. Langenbach-Belz (1976), Approximate formulae for the delay in the queueing system gi/g/1, in *Proceedings of International Teletraffic Congress*, vol. 8, p. 235-1, Melbourne.
- Lafforgue, A. (1977), Inventaire et examen des processus élémentaires de ruissellement et d'infiltration sur parcelles: Application à une exploitation méthodique des données obtenues sous pluies simulées, *Cah. O. R. S. T. O. M., Ser. Hydrol.*, 14, 299–344.
- Lampard, D. (1968), A stochastic process whose successive intervals between events form a first order Markov chain. I, *J. Appl. Probab.*, 5, 648–668.
- Langhans, C., G. Govers, J. Diels, A. Leys, W. Clymans, A. Putte, and J. Valckx (2011), Experimental rainfall–runoff data: Reconsidering the concept of infiltration capacity, *J. Hydrol.*, 399, 255–262.
- Le Bissonnais, Y., O. Cerdan, V. Lecomte, H. Benkhadra, V. Souchère, and P. Martin (2005), Variability of soil surface characteristics influencing runoff and interrill erosion, *Catena*, 62, 111–124.
- Lesschen, J., J. Schoorl, and L. Cammeraat (2009), Modelling runoff and erosion for a semi-arid catchment using a multi-scale approach based on hydrological connectivity, *Geomorphology*, 109, 174–183.
- Lindley, D. (1952), The theory of queues with a single server, *Math. Proc. Cambridge Philos. Soc.*, 48(2), 277–289.
- Michaelides, K., and A. Chappell (2009), Connectivity as a concept for characterising hydrological behaviour, *Hydrol. Processes*, 23, 517–522.
- Michaelides, K., and M. Wilson (2007), Uncertainty in predicted runoff due to patterns of spatially variable infiltration, *Water Resour. Res.*, 43, W02415, doi:10.1029/2006WR005039.
- Morbidelli, R., C. Corradini, and R. Govindaraju (2006), A field-scale infiltration model accounting for spatial heterogeneity of rainfall and soil saturated hydraulic conductivity, *Hydrol. Processes*, 20, 1465–1481.
- Morbidelli, R., C. Corradini, and R. Govindaraju (2007), A simplified model for estimating field-scale surface runoff hydrographs, *Hydrol. Processes*, 21, 1772–1779.
- Mueller, E., J. Wainwright, and A. Parsons (2007), Impact of connectivity on the modeling of overland flow within semiarid shrubland environments, *Water Resour. Res.*, 43, W09412, doi:10.1029/2006WR005006.
- Nahar, N., R. Govindaraju, C. Corradini, and R. Morbidelli (2004), Role of run-on for describing field-scale infiltration and overland flow over spatially variable soils, *J. Hydrol.*, 286, 36–51.
- Nielsen, D., J. Biggar, and K. Erh (1974), Spatial variability of field-measured soil-water properties, *Hilgardia*, 42(7), 215–259.
- Novak, A., and R. Watson (2009), Determining an adequate probe separation for estimating the arrival rate in an m/d/1 queue using single-packet probing, *Queueing Syst.*, 61, 255–272.
- Paige, G., J. Stone, D. Guertin, and L. Lane (2002), A strip model approach to parameterize a coupled Green-Ampt kinematic wave model, *J. Am. Water Resour. Assoc.*, 38, 1363–1377.
- Patin, J., E. Mouche, O. Ribolzi, V. Chaplot, O. Sengtahevhangoung, K. Latsachak, B. Souleuth, and C. Valentin (2012), Analysis of runoff production at the plot scale during a long-term survey of a small agricultural catchment in lao pdr, *J. Hydrol.*, 426, 79–92.
- Pilgrim, D., T. Chapman, and D. Doran (1988), Problems of rainfall-runoff modelling in arid and semiarid regions, *Hydrol. Sci. J.*, 33, 379–400.
- Prabhu, N. (1960), Some results for the queue with Poisson arrivals, *J. R. Stat. Soc., Ser. B*, 22, 104–107.
- Renard, P., and D. Allard (2011), Connectivity metrics for subsurface flow and transport, *Adv. Water Resour.*, 34, 168–196.
- Reynolds, J. (1975), The covariance structure of queues and related processes: A survey of recent work, *Adv. Appl. Probab.*, 7, 383–415.
- Ribolzi, O., J. Patin, L. Bresson, K. Latsachak, E. Mouche, O. Sengtahevhangoung, N. Silvera, J. Thiébaux, and C. Valentin (2011), Impact of slope gradient on soil surface features and infiltration on steep slopes in northern Laos, *Geomorphology*, 127, 53–63.
- Roberts, J., and F. Guillemin (1992), Jitter in atm networks and its impact on peak rate enforcement, *Perform. Eval.*, 16, 35–48.
- Russo, D., and E. Bresler (1981), Soil hydraulic properties as stochastic processes. I: An analysis of field spatial variability, *Soil Sci. Soc. Am. J.*, 45, 682–687.
- Saghafian, B., P. Julien, and F. Ogden (1995), Similarity in catchment response. 1: Stationary rainstorms, *Water Resour. Res.*, 31, 1533–1541.
- Sen, S., P. Srivastava, J. Dane, K. Yoo, and J. Shaw (2010), Spatial-temporal variability and hydrologic connectivity of runoff generation areas in a north Alabama pasture implications for phosphorus transport, *Hydrol. Processes*, 24, 342–356.
- Smith, W. (1953), On the distribution of queueing times, *Math. Proc. Cambridge Philos. Soc.*, 49, 449–461.
- Stauffer, D., and A. Aharony (1994), *Introduction to Percolation Theory*, CRC Press, London.
- Stidham, S. (1972), Regenerative processes in the theory of queues, with applications to the alternating-priority queue, *Adv. Appl. Probab.*, 4, 542–577.
- Stone, J., G. Paige, and R. Hawkins (2008), Rainfall intensity-dependent infiltration rates on rangeland rainfall simulator plots, *Trans. ASABE*, 51, 45–53.
- Tin, P. (1985), A queueing system with Markov-dependent arrivals, *J. Appl. Probab.*, 22, 668–677.
- Van Dijk, A., and L. Bruijnzeel (2004), Runoff and soil loss from bench terraces. 1: An event-based model of rainfall infiltration and surface runoff, *Eur. J. Soil Sci.*, 55, 299–316.
- Van Leeuwen, J., A. Löpker, and A. Janssen (2010), Connecting renewal age processes and m/d/1 processor sharing queues through stick breaking, *Stochastic Models*, 26(1), 141–163.
- Wainwright, J., and A. Parsons (2002), The effect of temporal variations in rainfall on scale dependency in runoff coefficients, *Water Resour. Res.*, 38, 1271, doi:10.1029/2000WR000188.
- Wainwright, J., L. Turnbull, T. Ibrahim, I. Lexartza-Artza, S. Thornton, and R. Brazier (2011), Linking environmental regimes, space and time: Interpretations of structural and functional connectivity, *Geomorphology*, 126, 387–404.
- Western, A., G. Blöschl, and R. Grayson (2001), Toward capturing hydrologically significant connectivity in spatial patterns, *Water Resour. Res.*, 37, 83–97.
- Wood, E., M. Sivapalan, and K. Beven (1986), Scale effects in infiltration and runoff production, International Association of Hydrological Sciences, IAHS-AISH publication, 156, 375–387.
- Wood, E., M. Sivapalan, K. Beven, and L. Band (1988), Effects of spatial variability and scale with implications to hydrologic modeling, *J. Hydrol.*, 102, 29–47, 1988.
- Woolhiser, D., R. Smith, and J. Giraldez (1996), Effects of spatial variability of saturated hydraulic conductivity on Hortonian overland flow, *Water Resour. Res.*, 32, 671–678.
- Yu, B., C. Rose, K. Coughlan, and B. Fentie (1997), Plot-scale rainfall-runoff characteristics and modeling at six sites in Australia and Southeast Asia, *Trans. ASAE*, 40, 1295–1303.